

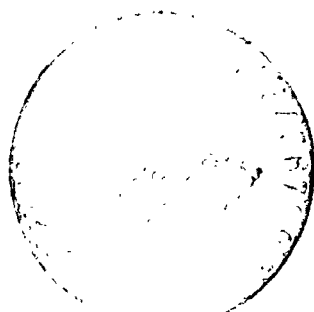
NASA Technical Memorandum 79234

ANALYTICAL CORE LOSS CALCULATIONS
FOR MAGNETIC MATERIALS USED IN
HIGH FREQUENCY HIGH POWER
CONVERTER APPLICATIONS

James E. Triner
Lewis Research Center
Cleveland, Ohio

(NASA-TM-79234) ANALYTICAL CORE LOSS N79-31499
CALCULATIONS FOR MAGNETIC MATERIALS USED IN
HIGH FREQUENCY HIGH POWER CONVERTER
APPLICATIONS Ph.D. Thesis - Toledo Univ. Unclass
(NASA) 103 p HC A06/MF A01 CSCL 09A G3/33 31988

August 1979



A Dissertation
entitled
**Analytical Core Loss Calculations for Magnetic Materials Used
in High Frequency High Power Converter Applications**

by
James E. Triner

as partial fulfillment of the requirements of
the Doctor of Philosophy Degree in
Engineering Science



Thomas A. Stewart
Advisor

Dean of the Graduate School

The University of Toledo
August 1979

An Abstract of
ANALYTICAL CORE LOSS CALCULATIONS FOR MAGNETIC MATERIALS USED
IN HIGH FREQUENCY HIGH POWER CONVERTER APPLICATIONS

James E. Triner

Submitted in partial fulfillment
of the requirements of the
Doctor of Philosophy Degree
in Engineering Science

The University of Toledo
August 1979

Analysis of future space energy needs has indicated a variety of missions requiring total energies exceeding those of past missions by two or three orders of magnitude (1 to 100 kW). A major part of such a system will be the power converter and inverter subsystems which process this energy to meet user requirements.

One of the major components within such a power subsystem is the magnetic device. This component is used for voltage and current transformation, input/output filter sections, parameter sensing, and semiconductor control. Recently, attention has been given to the different loss characteristics of magnetic devices observed under various excitation conditions.

This dissertation examines the basic magnetic properties under various operating conditions encountered in the state-of-the-art DC-AC/DC converters. Using a novel core excitation circuit, the basic B-H and loss characteristics of various core materials may be observed as a function of circuit configuration, frequency of operation, input voltage, and pulse-width modulation conditions. From this empirical data, a mathematical loss characteristics equation is developed to analytically predict the specific core loss of several magnetic materials under various waveform excitation conditions.

Previous magnetic core characteristics were observed using either a voltage source or a current source. For a core being excited in either of these modes, the voltage or current characteristics are observed as the independent variable. However, the excitation circuit used for this dissertation uses a high power wide bandwidth operational amplifier which senses the derivative of flux with time as the controlled parameter. Under these conditions flux is observed as the independent variable with voltage and current as the dependent variable.

Power measurements were obtained using a true RMS wide bandwidth wattmeter. The B-H loop characteristics were observed using an X-Y oscilloscope. This experimental excitation set-up allowed the magnetic characteristics to be measured and observed under square, ramp, and sinusoidal flux conditions.

Using this flux controlled excitation, magnetic core characteristics were developed for constant values of ramp flux and frequency. These characteristics will show the circuit designer for the first time the functional relationships between induction level and specific core loss as a function of the two key DC-DC converter operating parameters of input voltage and duty cycle.

Core excitations involving symmetric and asymmetric conditions for both sinusoidal and square wave waveforms were investigated analytically using three specific core loss calculation methods. Experimental data was used to compare the accuracy of these methods. The predicted and measured specific core losses were within 10 percent of each other for all conditions analyzed. This deviation is within the error band of the instrumentation. Therefore, these methods will analytically predict the specific core loss for any type of voltage excitation encountered in DC-AC/DC converter configurations using only one set of characteristic curves for the specific magnetic material, core configuration, and tape thickness.

ACKNOWLEDGMENTS

This research was supported by the National Aeronautics and Space Administration under RTOP 506-23-52 in the Power Electronics Branch at Lewis Research Center, Cleveland, Ohio.

I would like to express my deep appreciation to Dr. Thomas A. Stuart, my advisor, for his guidance and support throughout the course of my graduate work. His advice and assistance have brought insight to fundamental concepts and approaches.

I would also like to thank Mr. Irving G. Hansen, my colleague, for his technical assistance, and discussions at critical stages of my research; Mr. Fred F. Terdan for his management support during my graduate study leave; and Miss Gertrude R. Collins for her encouragement and guidance throughout my educational development program.

Finally, I would like to express my deepest admiration to my beloved wife, Jo-Ann. Her patience, understanding, and inspiration have been with me throughout the course of my graduate work.

James E. Triner

CONTENTS

	<i>Page</i>
ABSTRACT	ii
ACKNOWLEDGMENTS	iv
LIST OF FIGURES	vi
LIST OF TABLES	ix
I. INTRODUCTION	1
II. INVESTIGATION OF MAGNETIC CORE CHARACTERISTICS	6
2.1 Introduction	6
2.2 Review of Magnetics Equations	7
2.3 Calculation of Stacking Factor	12
2.4 General Experimental Set-Up	15
2.5 Source Impedance Effects	18
III. ANALYTICAL CORE LOSS CALCULATIONS	24
3.1 Introduction	24
3.2 Specific Core Loss Measurements	25
3.3 Separation of Loss Variables at Constant Frequency . .	29
3.4 Analytical Calculation Methods	35
IV. GENERAL CORE LOSS ANALYSIS	54
4.1 Introduction	54
4.2 Development of Computer Algorithm	55
4.3 Examples	61
V. CONCLUSIONS AND SUGGESTIONS FOR FUTURE RESEARCH	66
5.1 Conclusions	66
5.2 Applications in Power Electronics	69
5.3 Optimization of Tape Thickness	69
APPENDIXES	
A - SUMMARY OF SPECIFIC CORE LOSS DATA FOR FERRITE, SUPERMALLOY, AND SQUARE PERMALLOY 80 CORE MATERIALS	71
B - GLOSSARY OF SYMBOLS	85
LIST OF REFERENCES	87
BIOGRAPHY	91

LIST OF FIGURES

Figure		Page
1	Cross section microphotograph of 1/2, 1, 2, and 4 mil Supermalloy cut cores.	16
2	Comparisons of $i(t)$, $\phi(t)$, and $e(t)$ for ramp, square, and cosinusoidal reference voltages.	19
3	Detailed instrumentation system.	20
4	Relationships for $i(t)$, $\phi(t)$, and $\phi-I$ under voltage excitation.	22
5	Relationships for $i(t)$, $\phi(t)$, and $\phi-I$ under current excitation.	23
6	Comparisons of SCL characteristics for sinusoidal and square wave excitation with published data.	26
7	SCL characteristics for sinusoidal and square wave excitation with axes interchanged.	28
8	Comparisons of the four loss regions for the instantaneous B-H loop, $p(t)$, $i(t)$, and $e(t)$.	30
9	B-H loop as a function of $d\phi/dt$ for constant B_M and f .	31
10	Half cycle specific core loss per cycle versus $d\phi/dt$ with B_M as a parameter.	32
11	Comparison of B-H loop characteristics for constant and variable $d\phi/dt$ conditions with frequency and B_M as a constant.	34
12	Waveform excitation for a pulse width modulated square wave.	36
13	Specific core loss characteristics for cut 1/2 mil Supermalloy under duty-cycle conditions.	39
14	Comparison of calculated versus measured values of SCL for 1/2 mil Supermalloy as a function of duty cycle for a 1 kHz-3.9 volt pulse voltage.	40
15	SCL for f_{eq}^+ and f_{eq}^- with an excitation frequency (f_{ex}) of 1 kHz and 10 percent duty cycle.	43

Figure		Page
16	Comparison of calculated versus measured values of SCL as a function of duty cycle for a 1 kHz-3.9 volt pulse voltage.	45
17	Family of B-H loops and SCL characteristics based on $d\phi/dt$ as a parameter.	47
18	Comparison of calculated versus measured values of SCL as a function of duty cycle for a 1 kHz-3.9 volt pulse voltage.	52
19	Instantaneous energy characteristics.	53
20	An example to demonstrate the application of method 3 and the specific core loss equations.	59
21	Program listing for SCL analysis program.	60
22	Input-output formats for automated calculation of SCL of a magnetic material.	62
23	Waveform excitations for sinusoidal and nonsinusoidal conditions.	63
24	Comparison of calculated and measured results for specific core loss of 1/2 mil cut Supermalloy under sinusoidal excitation at 1000 Hz.	65
A.1	Specific core loss characteristics for 3B7 ferrite.	72
A.2..	Specific core loss characteristics for cut 1/2 mil Supermalloy.	73
A.3	Specific core loss characteristics for cut 1 mil Supermalloy.	74
A.4	Specific core loss characteristics for cut 2 mil Supermalloy.	75
A.5	Specific core loss characteristics for cut 4 mil Supermalloy.	76
A.6	Specific core loss characteristics for uncut 1/2 mil Supermalloy.	77
A.7	Specific core loss characteristics for uncut 1 mil Supermalloy.	78
A.8	Specific core loss characteristics for uncut 2 mil Supermalloy.	79

Figure		Page
A.9	Specific core loss characteristics for uncut 4 mil Supermalloy.	80
A.10	Specific core loss characteristics for uncut 1/2 mil Square Permalloy 80.	81
A.11	Specific core loss characteristics for uncut 1 mil Square Permalloy 80.	82
A.12	Specific core loss characteristics for 2 mil Square Permalloy 80.	83
A.13	Specific core loss characteristics for 4 mil Square Permalloy 80.	84

LIST OF TABLES

Table		Page
I	Comparison of four methods for determining stacking factor with published values.	12
II	Tabulation of the constant and exponent values used in Equation (4.4).	56
III	Tabulation of the constant and exponent values used in Equation (4.5).	57

CHAPTER I

INTRODUCTION

Magnetic materials offer the power electronics designer a wide range of magnetic characteristics (Ref. 1) from which he must select those materials applicable to his particular DC-AC/DC converter design. Like their semiconductor counterparts, magnetic devices display families of operating characteristics which are functions of frequency, temperature, basic material composition, fabrication techniques, and driving source impedance (Ref. 2). The interaction between these various functions may be explained by ferromagnetism, material properties, or domain wall movement (Ref. 3). However, for power electronics applications it is desirable to provide a set of magnetic characteristics which are easily understood and accurately predict the performance of a particular magnetic material when applied in a specific DC-AC/DC converter configuration.

This dissertation examines the B-H and loss characteristics of several magnetic materials used in present state-of-the-art power processing circuits. The effects of variables such as frequency, voltage level, voltage waveforms, and modulation upon the inherent material characteristics are explored using only externally measurable quantities.

Traditionally derived core loss data are presented as a function of flux density with frequency as a parameter. In general, hard experimental data is taken with sinusoidal voltage excitation of 60 or

400 hertz. The family of characteristic core loss curves are then generated by using a mathematical formula such as that proposed by Legg (Ref. 4). However, this method is only valid for low values of flux density. Only recently has attention been given to the different loss characteristics of magnetic materials observed between sinusoidal and square-wave excitation conditions at 10,000 hertz (Ref. 5). In the past, only circuits having similar excitation conditions could utilize these loss characteristics. Newly available state-of-the-art instrumentation equipment, and mathematical techniques developed in this dissertation allow the power electronics designer to calculate the specific core loss for various nonsinusoidal, and asymmetrical square wave excitation conditions using only these loss characteristics.

The square wave B-H loop and associated core loss characteristics may be observed in a unique manner by means of an excitation source in which the flux rate of change ($d\phi/dt$) is observed as the independent variable, and the power loss is measured using a wide bandwidth (DC-300 K Hz) wattmeter. This excitation circuit, which is fully described in Chapter II, allows the control of an additional variable, $d\phi/dt$, rather than just the driving frequency as is the case for all previous sinusoidal core loss measurements. If the excitation is restricted to that of a constant frequency square wave voltage having a variable duty-cycle, the $d\phi/dt$ effects may then be determined for various constant values of B_M independent of frequency. For the first time, the distribution of the B-H loop area is shown to be dependent upon the positive and negative $d\phi/dt$ ramp rates. The wideband wattmeter allows core loss data to be accurately measured under these conditions. This procedure allows a true separation of the variables $d\phi/dt$, frequency,

and B_M . This data is then used to develop the functional relationships of hysteresis loss with B_M , and eddy current loss with B_M and $d\phi/dt$.

Sinusoidal core loss characteristics for a particular magnetic material and lamination thickness are generally shown with flux density as the independent variable, specific core loss as the dependent variable, and frequency as a parameter (Ref. 6). Data collected with the new excitation circuit is based upon values of constant $d\phi/dt$ which corresponds with square wave excitation. The core loss characteristics are shown with frequency as the independent variable, specific core loss as the dependent variable, and $d\phi/dt$ and flux density as parameters.

In Chapter III these loss characteristics, the B-H loop behavior, and the instantaneous power waveshapes observed for the various waveforms are used to develop three methods which analytically predict the specific core loss for magnetic materials. A pulse width modulated square wave with a 10 to 50 percent duty cycle is then used to compare the experimental and analytical accuracy of each method.

The first method, which is similar to the sinusoidal analysis techniques already in common use, allows the specific core loss to be calculated directly from the characteristics knowing the maximum flux density (B_M) and the frequency of operation. To calculate the value of B_M for the excitation pulse, the cross sectional area of the core, number of turns, excitation voltage level, and pulse width must be known. In the second method, the specific core loss is calculated by using $d\phi/dt$ and an "equivalent" excitation frequency.

The value of $d\phi/dt$ is directly proportional to the input voltage

and inversely proportional to the number of turns on the core. The "equivalent" frequency is inversely proportional to twice the pulse width. The third method is developed as an extension of the second method. The excitation pulse is subdivided into a discrete number of time steps. The average voltage level is determined for each time step. This voltage level along with the number of turns on the core correspond to an incremental value of $d\phi/dt$. This corresponds to an incremental loss at some "equivalent" frequency. The total specific core loss is then the summation of these incremental losses divided by total period. These methods cover the functional relationship between induction level and specific core loss as a function of excitation voltage level and duty-cycle characteristics.

The concepts developed for the square wave in the third method are extended to analyze other types of waveforms in Chapter IV. A general equation form is used to relate the specific core loss to $d\phi/dt$, and the equivalent frequency of the excitation. The coefficient and exponents that relate these variables are dependent on the magnetic material, and the tape thickness, or grain size. Using this general equation a computer algorithm is then developed which automates the analysis procedure. Analytical and experimental results are compared for sinusoidal and nonsinusoidal examples using three different core materials and configurations. As a final example the specific core loss characteristics for 1/2 mil Supermalloy material under sinusoidal excitation are generated using the characteristic equation for square wave excitation and the computer algorithm.

Finally, Chapter V presents the conclusions of this work and suggestions for future research in this area. Specific core loss data

for several magnetic tape materials and ferrite are presented in Appendix A. A glossary of symbols and their associated units are in Appendix B.

CHAPTER II

INVESTIGATION OF MAGNETIC CORE CHARACTERISTICS

2.1 Introduction

The analytical core loss calculation methods developed in this dissertation are based upon the core characteristics observed under controlled flux excitation. The width of the B-H loop was found to be a function of both the flux rate of change ($d\phi/dt$) and the maximum flux density (B_M).

In all the specific core loss (SCL) characteristics presented, both positive and negative values of $d\phi/dt$ were held constant over one cycle. These $d\phi/dt$ conditions allow symmetrical square wave voltage excitation of the magnetic material under test. With the data recorded in this manner Faraday's Law (Ref. 7) is then used to calculate the $d\phi/dt$ value directly using the excitation voltage level, and the number of turns on the core. In an actual DC-DC converter application the excitation voltage level is the input voltage being applied to a particular magnetic device. Using the SCL characteristics as developed by this method, the power electronics designer may for the first time calculate the SCL for the magnetic device directly knowing only the input voltage, duty cycle, and the frequency of operation.

If the effective cross sectional area (A_e) is known, then the flux density in the magnetic material may be calculated. To accurately determine the value of A_e the physical cross sectional area of the core (A_C) and the stacking factor (SF) must be known. Four methods of

determining the SF value for cut cores are presented in this section. The results of these methods indicate that the SF value for this core configuration can be measured to within 5 percent of its actual value.

The excitation circuit allows three different source configurations to be simulated. By using voltage feedback the excitation source represents a voltage source. If current feedback is used, the excitation source represents a current source. When flux feedback is used, the observed magnetic characteristics become independent of source impedance. Thus, true sinusoidal or square wave voltage excitation can be easily generated. This excitation circuit eliminates many of the problems encountered with conventional square wave excitation sources.

The instrumentation system was designed to efficiently collect the core loss data required for the development of the desired SCL characteristics. The system was also used to run the desired experimental waveshapes against which the analytical core loss calculations were then compared. The instrumentation system utilizes a Phillips PM 3252 multiplying oscilloscope for observing instantaneous $p(t)$ waveshapes. A Tektronix 7704 mainframe is used to simultaneously observe $e(t)$, $i(t)$, $p(t)$, $\phi(t)$, and the instantaneous B-H loop.

2.2 Review of Magnetics Equations

All available presentations of specific core loss characteristics display flux density as the independent variable, SCL as the dependent variable, and frequency as a parameter. To use this data requires that the A_e of the core be accurately known. This parameter is not always readily available and is inaccurate in most of the published data. However, for the majority of power electronic applications the input

voltage, frequency of operation, number of turns, and duty cycle conditions of a magnetic device are known.

In a magnetic device a time-varying magnetic field produces a voltage which may establish a current in a suitable closed circuit. Faraday's law (Ref. 7), expressed in the CGS electromagnetic system of units, shows the relationship between this changing magnetic field and the induced voltage:

$$e(t) = -(d\phi/dt) \times 10^{-8} \text{ volts} \quad (2.1)$$

The minus sign indicates that the voltage is in such a direction as to produce a current whose flux, if added to the original flux, would reduce the magnitude of the voltage. This statement that the induced voltage acts to produce an opposing flux is known as "Lenz's law."

If the magnetic field is coupled by an N turn conductor, then

$$e(t) = -N(d\phi/dt) \times 10^{-8} \text{ volts} \quad (2.2)$$

By use of equation (2.2), transformer equations for both sinusoidal and square wave voltage excitation may be derived. If $e(t)$ represents a square wave of voltage, then $\phi(t)$ would be a ramp function with its slope proportional to the volts/turn ratio. Over one half cycle ($0 \leq t \leq T/2$), $e(t)$ has a constant value E . For the same interval $\phi(t)$ goes from $-\phi_M$ to $+\phi_M$. The standard form of the transformer equation for square wave excitation is obtained by integrating equation (2.2) over this half cycle interval:

$$\int_{\phi=-\phi_M}^{\phi=+\phi_M} d\phi = - \frac{E \times 10^8}{N} \int_{t=0}^{t=T/2} dt$$

$$\left[\begin{array}{c} +\phi_M \\ -\phi_M \end{array} \right] = - \frac{E \times 10^8}{N} t \left[\begin{array}{c} T/2 \\ 0 \end{array} \right]$$

$$2\phi_M = - \frac{E \times 10^8 T}{2N}$$

Rearranging terms

$$E = -4\phi_M T^{-1} N \times 10^{-8} \text{ volts} \quad (2.3)$$

Since

$$\phi_M = B_M A_e = B_M A_c S F \text{ maxwells} \quad (2.4)$$

and

$$f = T^{-1} \text{ Hz} \quad (2.5)$$

Substituting (2.4) and (2.5) into (2.3):

$$E = -4B_M A_c S F f N \times 10^{-8} \text{ volts} \quad (2.6)$$

If $e(t)$ represents a sinusoidal voltage, then $\phi(t)$ would be a cosine function. Over one half cycle ($0 \leq t \leq \pi/\omega$), $e(t)$ is a sine wave with an amplitude of $\sqrt{2} E$. For the same interval $\phi(t)$ goes from $-\phi_M$ to $+\phi_M$. The standard form of the transformer equation for sinusoidal excitation is obtained by integrating equation (2.2) over this interval:

$$\int_{\phi=-\phi_M}^{\phi=+\phi_M} d\phi = - \frac{\sqrt{2} E \times 10^8}{N} \int_0^{\pi/\omega} \sin \omega t dt$$

$$\left[\begin{array}{c} +\phi_M \\ -\phi_M \end{array} \right] = + \frac{\sqrt{2} E \times 10^8}{\omega N} \cos \omega t \Big|_0^{\pi/\omega}$$

$$2\phi_M = - \frac{2\sqrt{2} E \times 10^8}{\omega N}$$

Rearranging terms

$$E = -(\sqrt{2})^{-1} \phi_M \omega N \times 10^{-8} \text{ volts} \quad (2.7)$$

Since

$$\omega = 2\pi f \text{ rad-sec}^{-1} \quad (2.8)$$

Substituting (2.4) and (2.8) into (2.7)

$$E = -(\sqrt{2})^{-1} B_M A_c SF 2\pi f N \times 10^{-8} \text{ volts}$$

or

$$E = -4.44 B_M A_c SF f N \times 10^{-8} \text{ volts} \quad (2.9)$$

By using Equation (2.9) the flux density for a given excitation condition may be calculated. Once this value is known, published SCL data for sinusoidal excitation may be used to directly determine the SCL for a particular magnetic material. To the author's knowledge, published data for square wave excitation conditions is essentially nonexistent. However, using the methods described in this dissertation square wave characteristics may be easily obtained. The square-wave SCL characteristics have a distinct advantage over the sine SCL characteristics because the effects of an additional parameter $d\phi/dt$ may also be examined using the same set of characteristics. In addition, by rearranging the representative axes with frequency as the independent variable, and SCL as the dependent variable, with B_M and $d\phi/dt$ as parameters, the characteristics become easier to use. In Chapter 4 the square wave SCL characteristics will be used to gen-

erate the sinusoidal SCL characteristics directly.

The SCL characteristics shown in Appendix A represent the total core loss as a function of frequency. If the energy loss is examined on a per cycle basis (Ref. 8), the effects of $d\phi/dt$, B_M , and frequency may be observed. The energy loss associated with the hysteresis loop is readily determined using Warburg's law (Ref. 9):

$$W_h = \frac{1}{4\pi} \oint H dB \quad \text{watt-sec} \quad (2.10)$$

In the instrumentation system used, the input current to the core under test was observed as the abscissa, and the integral of the input voltage was observed as the ordinate. Using Equation (2.2), and the chain rule, Equation (2.10) may be rewritten in terms of the input voltage $e_i(t)$ and the input current $i_i(t)$:

$$\begin{aligned} W_h &= \frac{1}{4\pi} \int_{t=0}^{t=T} H \frac{dB}{dt} \cdot dt \\ &= -\frac{1}{4\pi} \int_{t=0}^{t=T} \left[NL^{-1} i_i(t) \right] \left[A_e^{-1} N^{-1} e_i(t) \right] dt \\ W_h &= -(4\pi L A_e)^{-1} \int_{t=0}^{t=T} p_i(t) dt \quad \text{watt-sec} \end{aligned} \quad (2.11)$$

Equation (2.11) indicates that the area enclosed by the observed B-H loop is proportional to the energy (hysteresis) loss per cycle.

Separation of the eddy current, hysteresis, and anomalous loss components (Refs. 10 to 13) of the total core loss has been explored using only sinusoidal excitation methods. However, by using pulse width modulated square wave excitation techniques a direct separation of loss variables may be accomplished.

2.3 Calculation of Stacking Factor

Four different methods were used to determine the stacking factor of the cut cores used for this dissertation. The oil displacement method and the cross sectional scan method used the physical properties of the core to determine the stacking factor value. The sinusoidal and square wave excitation methods used the electrical properties of the core, and an assumed value for the maximum flux density. Supermalloy cut cores with 1/2, 1, 2, and 4 mil tapes were used and the stacking factors obtained using these four methods were compared with published values. Table I shows the results of this comparison. The four methods used are discussed in detail below:

Displacement method. - In this method Archimedes' principle (Ref. 14) is used to determine the true displacement volume of the core. First, the core is weighed in air:

$$W_{\text{core}_{\text{air}}} = \rho_{\text{core}} V_{\text{Fe}}$$

or

$$V_{\text{Fe}} = W_{\text{core}_{\text{air}}} (\rho_{\text{core}})^{-1}$$

TABLE I. - COMPARISON OF FOUR METHODS FOR DETERMINING
STACKING FACTOR WITH PUBLISHED VALUES

Tape thickness, mils	Displacement method	Sine ex. method	Square ex. method	Cross sec. method	Published value
0.5	0.865	0.885	0.843	0.914	0.80
1.0	.888	.928	.856	.895	.90
2.0	.932	.965	.934	.941	.92
4.0	.927	1.00	.934	.967	.94

Next the core is weighed in an oil of known density. The displacement weight ΔW is then

$$\Delta W = W_{\text{core}_{\text{air}}} - W_{\text{core}_{\text{oil}}} = \rho_{\text{oil}} V_{\text{core}}$$

or

$$V_{\text{core}} = \Delta W (\rho_{\text{oil}})^{-1}$$

The stacking factor is the ratio of the air volume of the core to the oil volume of the core:

$$\text{Stacking factor} = \frac{V_{\text{Fe}}}{V_{\text{core}}}$$

Example:

Core: 1/2 mil Supermalloy cut core $\rho_{\text{core}} = 8.7 \text{ gm-cm}^{-3}$

$W_{\text{core}_{\text{air}}} = 345 \text{ grams}$ $\rho_{\text{oil}} = 0.928 \text{ gm-cm}^{-3}$

$W_{\text{core}_{\text{oil}}} = 302.5 \text{ grams}$ $\Delta W = 42.5 \text{ grams}$

$$\text{Stacking factor} = (345/8.7)/(42.5/0.928) = 0.865$$

Excitation methods. - These are indirect methods in which the saturation flux density is used to determine A_e . The core is excited until the current waveform indicates that the core is in the saturation region. Then the excitation voltage level, and frequency are measured. Using the transformer equations derived in Section 2.2, A_e may be calculated:

For the sine wave:

$$A_e = E(4.44 B_M f N \times 10^{-8})^{-1}$$

For the square wave:

$$A_e = E(4B_M f N \times 10^{-8})^{-1}$$

The stacking factor is expressed as

$$\text{Stacking factor} = A_e A_c^{-1}$$

These values are measured at several frequencies and an average stacking factor value is calculated.

Example:

Core: 1/2 mil Supermalloy	A_c : 2.277 cm^2
N: 10 turns	B_M : 7.2 KGauss

For sine wave data:

f, hertz	e, volts	A_e , cm^2
600	3.86	2.01
700	4.48	2.00
800	5.13	2.00
900	5.83	2.02
1000	6.5	2.03

$$\bar{A}_e = 2.01 \text{ cm}^2$$

$$\text{Stacking factor} = 2.01/2.277 = 0.883$$

For square wave data:

f, hertz	e, volts	A_e , cm^2
600	3.36	1.94
700	3.86	1.91
800	4.41	1.91
900	5.07	1.95
1000	5.44	1.89

$$\bar{A}_e = 1.92 \text{ cm}^2$$

$$\text{Stacking factor} = 1.92/2.277 = 0.843$$

Cross sectional scan. - In this method a microphotograph of the core cross section is used to determine the stacking factor value. An

optical micrometer is used to measure the adhesive thickness and the actual tape thickness. Since the tape width is constant, the stacking factor is the ratio of the tape thickness to the tape plus adhesive thickness width or

$$\text{Stacking factor} = T_{\text{tape}} / (T_{\text{tape}} + T_{\text{adhesive}})$$

If these values are measured at several points across the core surface, and average stacking factor value may be calculated. In Figure 1 the microphotographs for the four tape thicknesses are shown.

Example:

Core: 1/2 mil Supermalloy

Tape thickness, in.	Adhesive thickness, in.
0.000609	0.00003125
.000578	.0000375
.000537	.0000375
.	.
.	.
.	.
0.000546	0.0000468

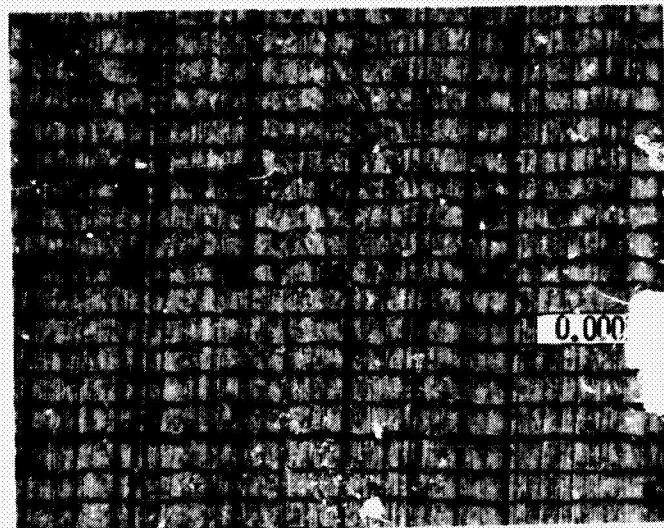
$$\bar{T}_{\text{tape}} = 0.000546 \text{ (in.)} \quad \bar{T}_{\text{adhesive}} = 0.00005125 \text{ (in.)}$$

$$\text{Stacking factor} = 0.000546 / (0.000546 + 0.00005125)$$

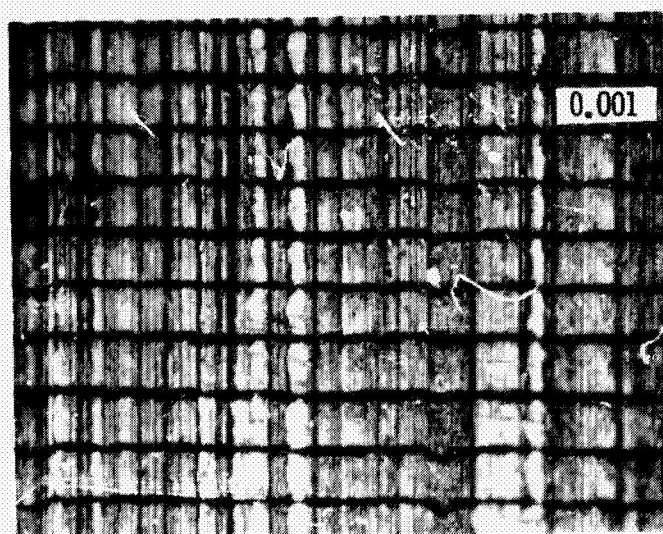
$$= 0.914$$

2.4 General Experimental Set-Up

Previous excitation methods have used feedback control schemes (Ref. 15) to reduce the harmonic content of the sinusoidal excitation by controlling the apparent source impedance. For this work, feedback control is used to achieve the desired voltage excitation. If a square wave voltage is required, a triangular reference voltage is used. If an impulse voltage is required, a square wave reference voltage is used.



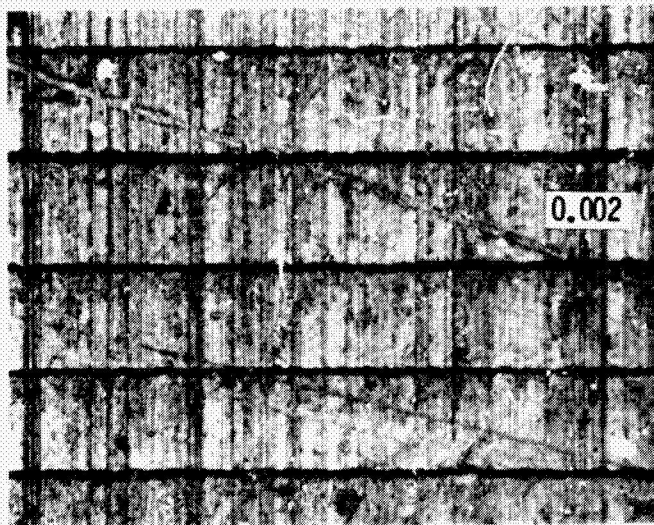
(a) 1/2 mil Supermalloy tape.



(b) 1 mil Supermalloy tape.

Figure 1.- Cross section Microphotographs of 1/2, 1,
and 4 mil Supermalloy cut cores.

PRINTED IN U.S.A.
ON ECON. QUALITY



(c) 2 mil Supermalloy tape.



(d) 4 mil Supermalloy tape.

Figure I.- Concluded.

ORIGINAL PAGE IS
OF POOR QUALITY

And, if sinusoidal voltage excitation is required, a cosinusoidal reference is used. Figure 2 shows the voltage, current, and flux relationships for each of these flux reference conditions.

The complete instrumentation system is shown in Figure 3. A high power operational amplifier was designed which allowed the option of selecting either voltage, current, or the integral of voltage (flux) as the feedback parameter. A Wavetek model 146 signal generator was used to generate the desired symmetrical flux waveshape. An ICL 8038 multifunction integrated circuit was used to generate the asymmetrical square and sinusoidal reference waveforms. The excitation frequency was measured with a Hewlett-Packard 5212A electronic counter. A Clarke-Hess model 225 wideband wattmeter (0 to 300 kHz) was used to measure the average input power into the core under test. This instrument allows the power delivered by a 100 kHz square wave to be normally measured to within 2 percent. The internal current shunt in the wattmeter displays the input current signal used for several measurements. A Phillips PM 3252 multiplying oscilloscope was also used to obtain the instantaneous $p_i(t)$ in the core. The input voltage to the core was measured with a Hewlett-Packard 3403C true RMS voltmeter. The Tektronix 7704 oscilloscope was used to observe $i_i(t)$, $e_i(t)$, $\phi(t)$, $p_i(t)$ as well as the instantaneous B-H loop of the core under test.

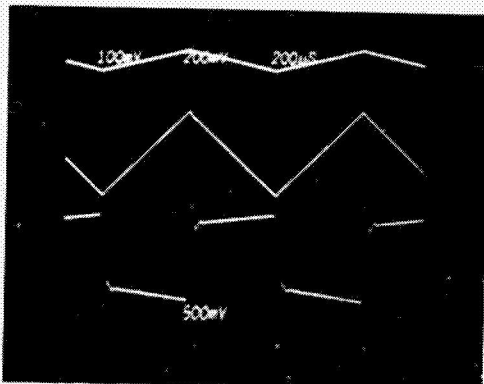
2.5 Source Impedance Effects

Source impedance effects discussed in the literature (Refs. 16 and 17) show that the width of the B-H loop to be dependent upon the driving source impedance. By changing the feedback parameter on the operational amplifier, a voltage source (R_L) or a current source

$i(t) = 0.5 \text{ A/Div}$

$\varphi(t) = 1050 \text{ Max/Div}$

$e(t) = 0.5 \text{ V/Div}$

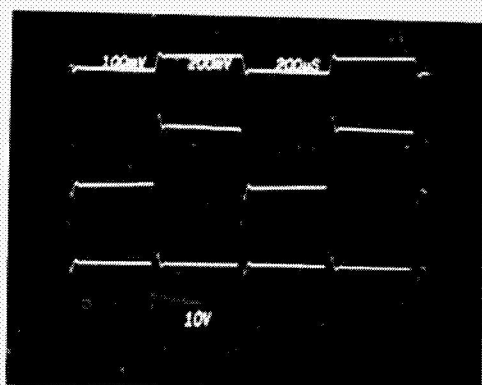


(a) Ramp $d\varphi/dt \rightarrow$ square voltage.

$i(t) = 0.5 \text{ A/Div}$

$\varphi(t) = 1050 \text{ Max/Div}$

$e(t) = 0.5 \text{ V/Div}$

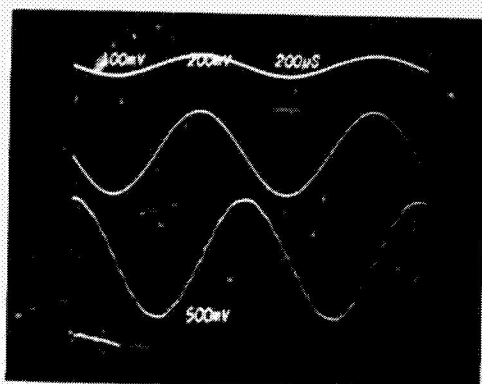


(b) Square $d\varphi/dt \rightarrow$ impulse voltage.

$i(t) = 0.5 \text{ A/Div}$

$\varphi(t) = 1050 \text{ Max/Div}$

$e(t) = 10 \text{ V/Div}$



(c) Sine $d\varphi/dt \rightarrow$ cosine voltage.

Figure 2. - Comparisons of $i(t)$, $\varphi(t)$, and $e(t)$ for ramp, square, and cosinusoidal reference voltages.

ORIGINAL PAGE IS
OF POOR QUALITY

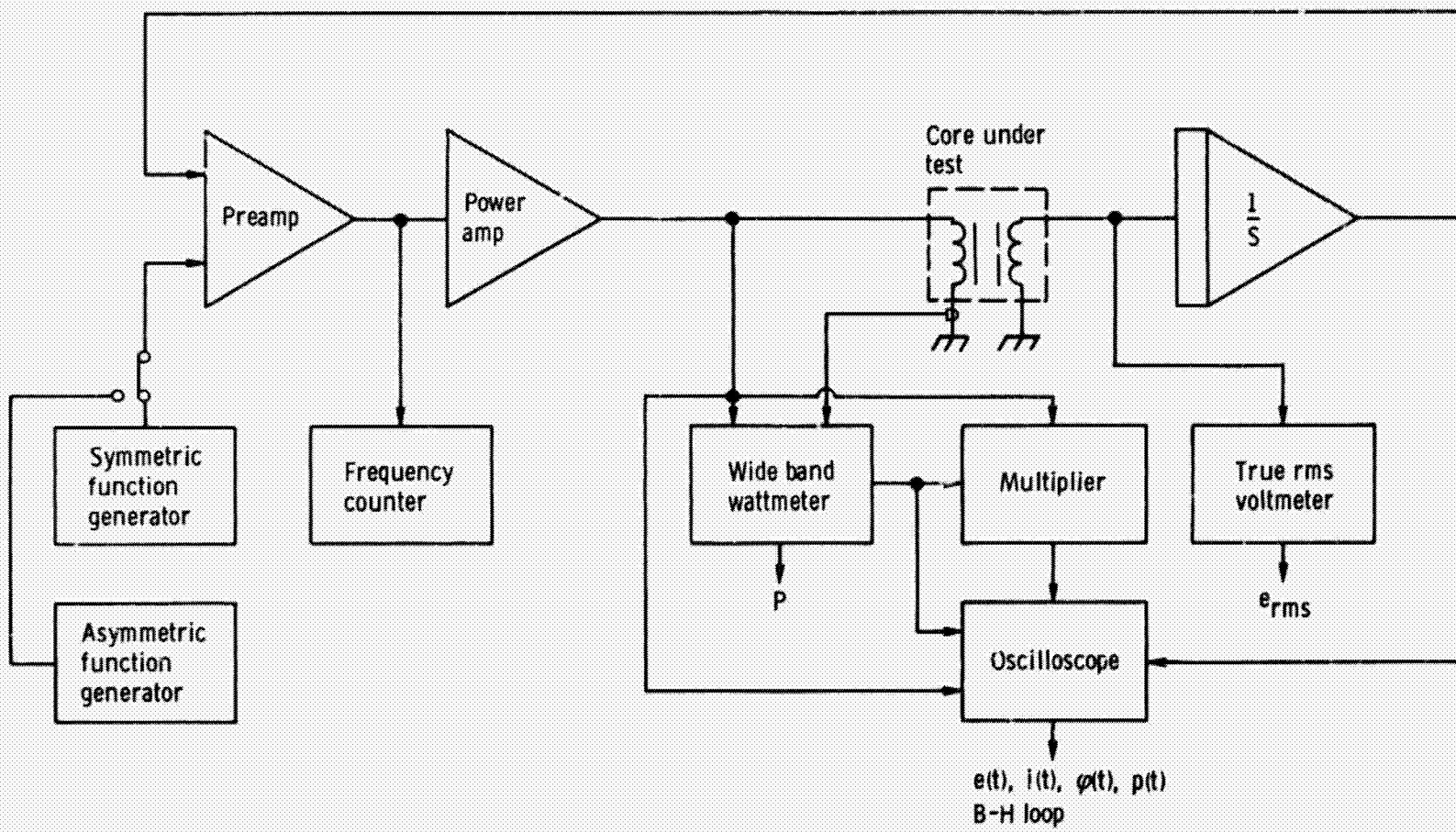


Figure 3. - Detailed instrumentation system.

($R_s \gg R_L$) may be simulated. The flux, current, and B-H loop characteristics for these two source configurations are shown in Figures 4 and 5. For the same B_M conditions, the width of the B-H loop is wider if the core is being driven by a current source. However, if the flux is observed for these two source conditions it can be seen that for sinusoidal current conditions, the flux approaches a square wave. This is a condition having a higher $d\phi/dt$ rate in the core than that realized under sinusoidal voltage conditions. Therefore, the observed B-H width is really a function of $d\phi/dt$ rather than being dependent upon source impedance.

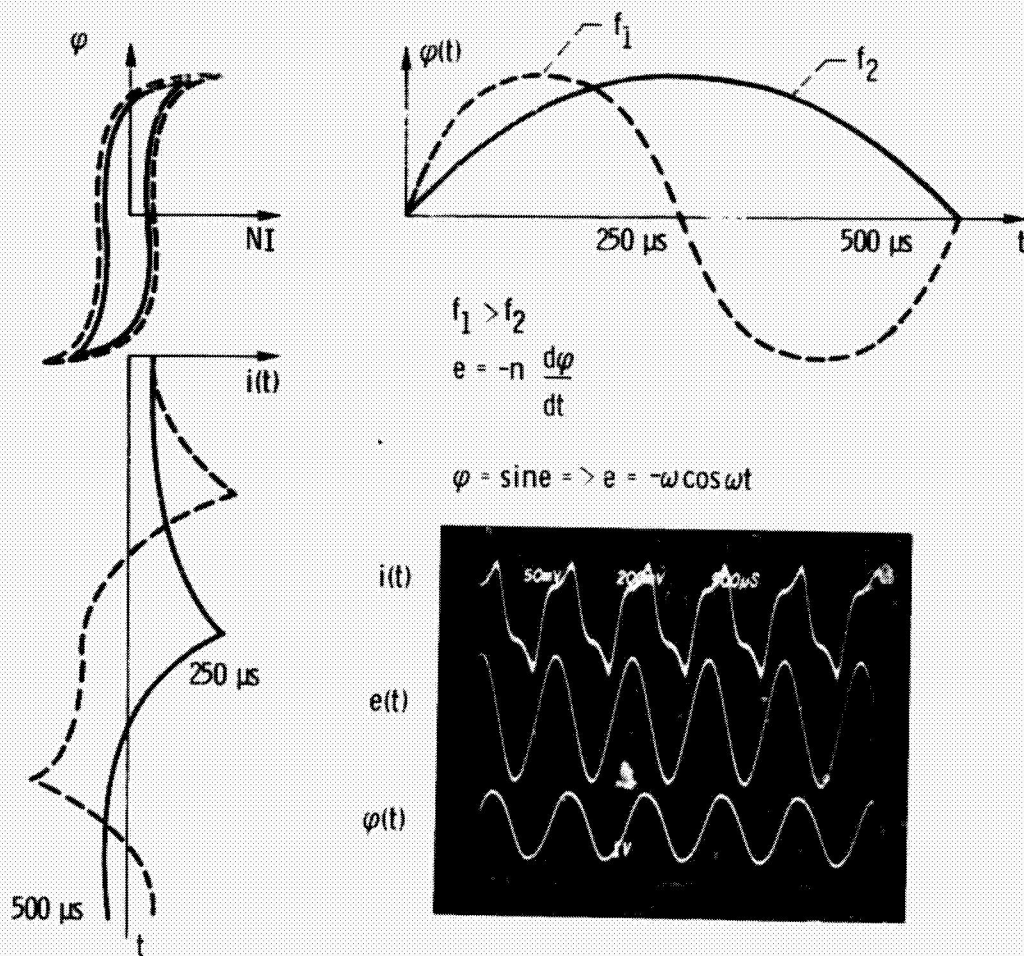


Figure 4. - Relationships for $i(t)$, $\phi(t)$, and ϕ - I under voltage excitation.

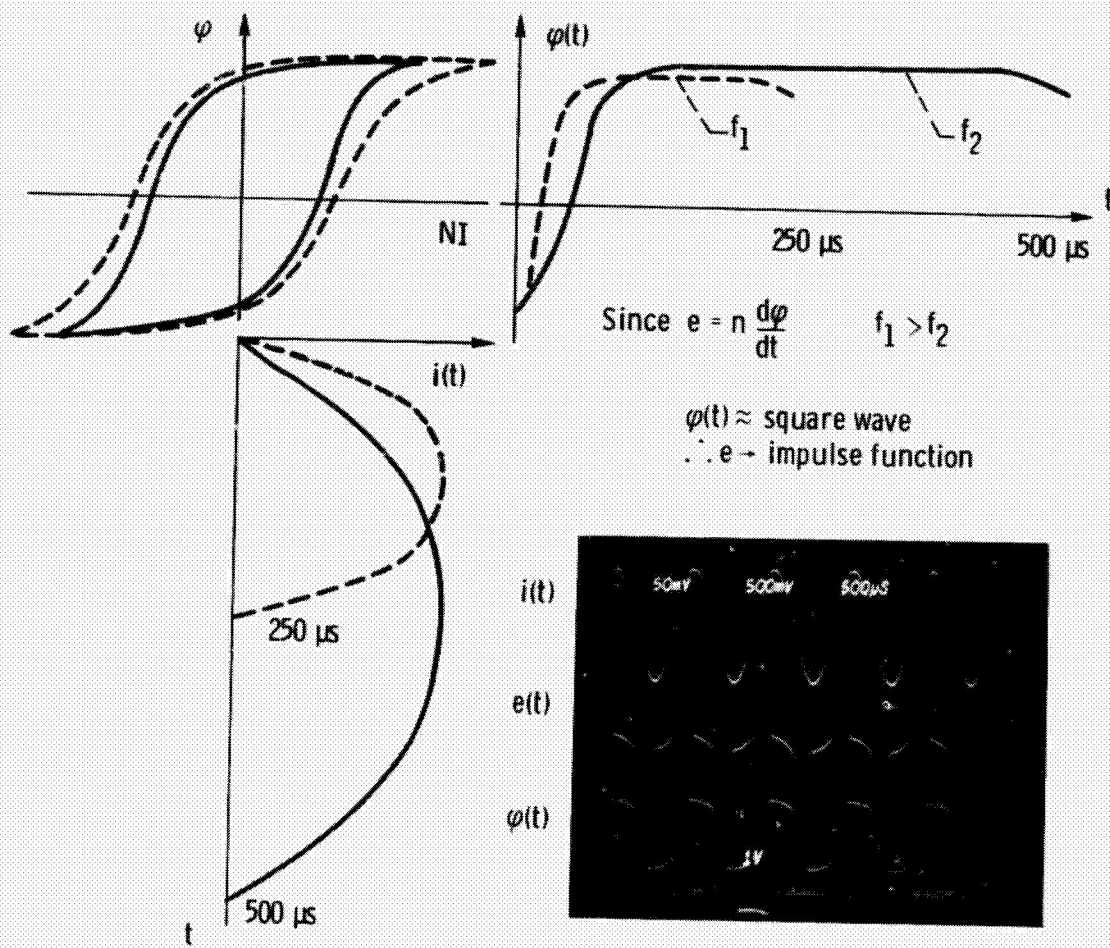


Figure 5. - Relationships for $i(t)$, $\phi(t)$, and ϕ -I under current excitation.

CHAPTER III

ANALYTICAL CORE LOSS CALCULATIONS

3.1 Introduction

Analytical prediction of core loss in magnetic materials is important from both an economic (Ref. 18) and an engineering design (Ref. 19) standpoint. Accurate prediction allows design tradeoffs to be made between the areas of weight, efficiency, and performance. In addition new circuit developments employing magnetic devices may be more fully analyzed without hardware fabrication. Early work (Ref. 20) at frequencies of up to 200 kHz was aimed at measuring the magnetic properties of iron. Separation of core loss into its specific components of eddy current, static hysteresis, and anomalous loss has been examined in great depth (Refs. 21 to 23) for low frequency (<1 kHz) sinusoidal excitations.

With the growth of power electronics to higher power levels and the employment of new converter techniques, the need to understand the properties of magnetic materials under nonsinusoidal conditions is arising. Recent comparisons between sinusoidal and square wave core loss (Ref. 5) indicate a lack of theory to predict the loss difference observed between these two excitations. However, if the dependence of the B-H characteristics upon the flux conditions described in Section 2.5 is expanded, the loss characteristics for these two excitations may be qualitatively observed, and predicted using easily obtained data.

In this chapter a comparison between sinusoidal and square wave

core loss is made. The results are shown to be consistent with the values published in the literature. Next, pulse width modulated square wave excitation is used as an analytical tool to achieve a true separation between the $d\phi/dt$ and B_M effects. Finally, three methods are developed to analytically predict the SCL for square wave excitation. These results are compared with experimentally measured results obtained under the same excitation conditions.

3.2 Specific Core Loss Measurements

To generate the SCL characteristics under square wave excitation for the magnetic materials studied, data was taken by holding $d\phi/dt$ constant and varying the excitation frequency. The power input to the core was measured at regular frequency intervals. The actual values for SCL in watts/pound and B_M in gauss were calculated from the raw data using the following formulas:

$$\frac{\text{Measured core loss in watts}}{\text{Measured core weight in pounds}} = \text{SCL(W/lb)} \quad (3.1)$$

$$\frac{\text{Measured } e_{\text{rms}} \text{ in volts}}{kA_c \text{ SFf } N \times 10^{-8}} = B_M(\text{gauss}) \quad (3.2)$$

where

$k = 4$ for square wave excitation

$= 4.44$ for sinusoidal excitation

Figure 6 shows the specific core loss for 1/2 mil cut Supermalloy under both sinusoidal (Fig. 6(a)) and square wave (Fig. 6(b)). In addition, comparisons are made with published sinusoidal data for these two excitation conditions. The major difference between the published and measured values for sinusoidal excitation may be accounted for by

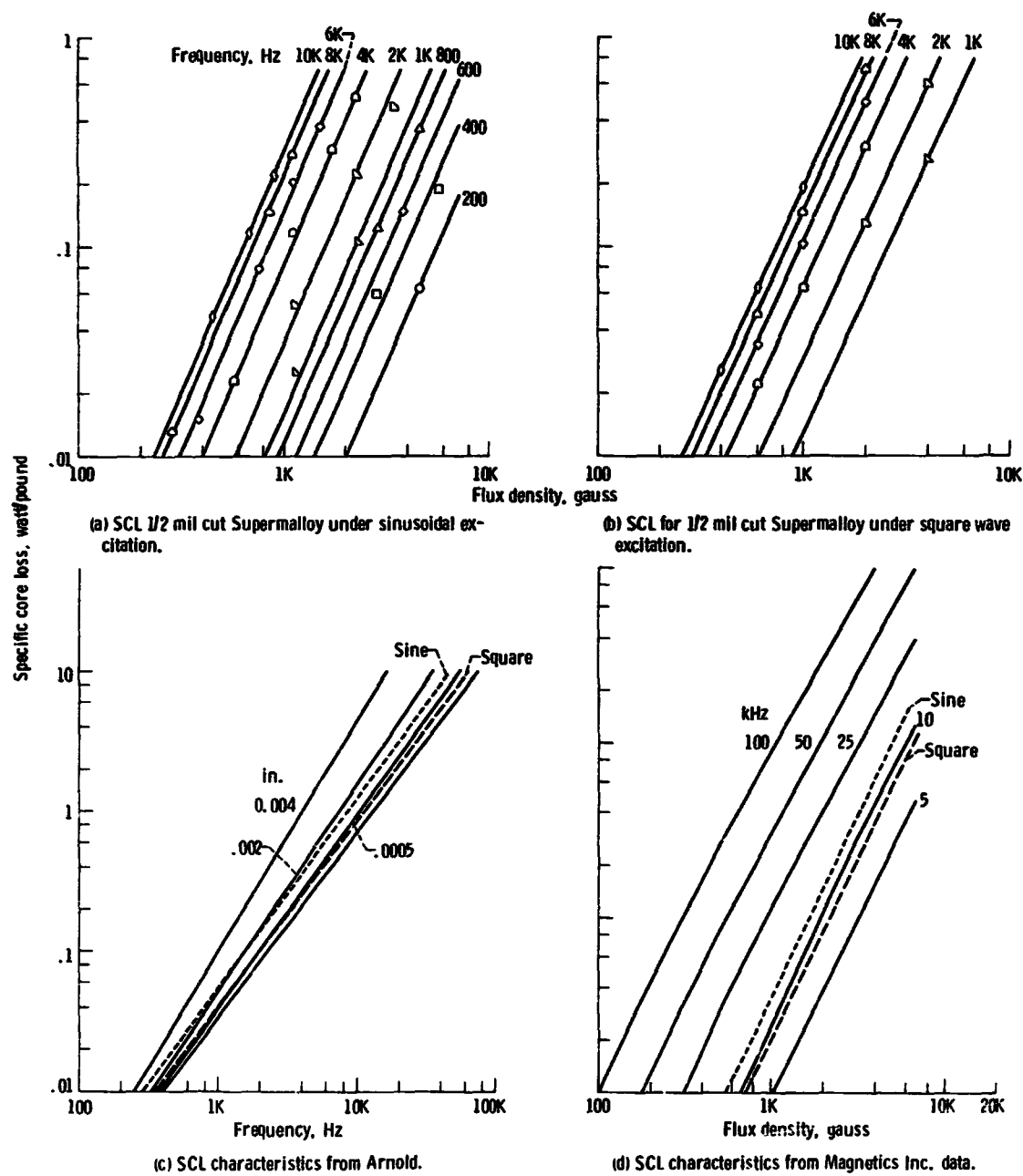


Figure 6. - Comparison of SCL characteristics for sinusoidal and square wave excitation with published data.

several factors:

Probable accuracy of the published data
Accuracy of the core loss measurement
Limited raw core loss data available
Driving source impedance
Measurement of actual excitation voltage level
Value assumed for stacking factor
Batch variations for the magnetic material
Actual lamination thickness

It is interesting to note that for equal values of B_M the SCL for sinusoidal excitation is greater than for square wave excitation.

Example:

$B_M = 2k$ gauss frequency = 1 kHz
SCL (sine) = 0.078 W/lb
SCL (square) = 0.058 W/lb

From these results it can be seen that the SCL for square wave excitation is approximately 26 percent less than the SCL for sinusoidal excitation. This result is consistent with previous observations (Ref. 5) which compared loss conditions for these two excitations.

To aid in the development of methods for specific loss calculations, data is replotted with the frequency and flux density axes interchanged. Figure 7(a) shows SCL versus frequency with B_M as a parameter for cut 1/2 mil Supermalloy under sinusoidal excitation. Figure 7(b) shows these characteristics for square wave excitation. For square wave excitation conditions, $d\phi/dt$ was held constant as well as frequency. This allowed the additional parameter of $d\phi/dt$ to be

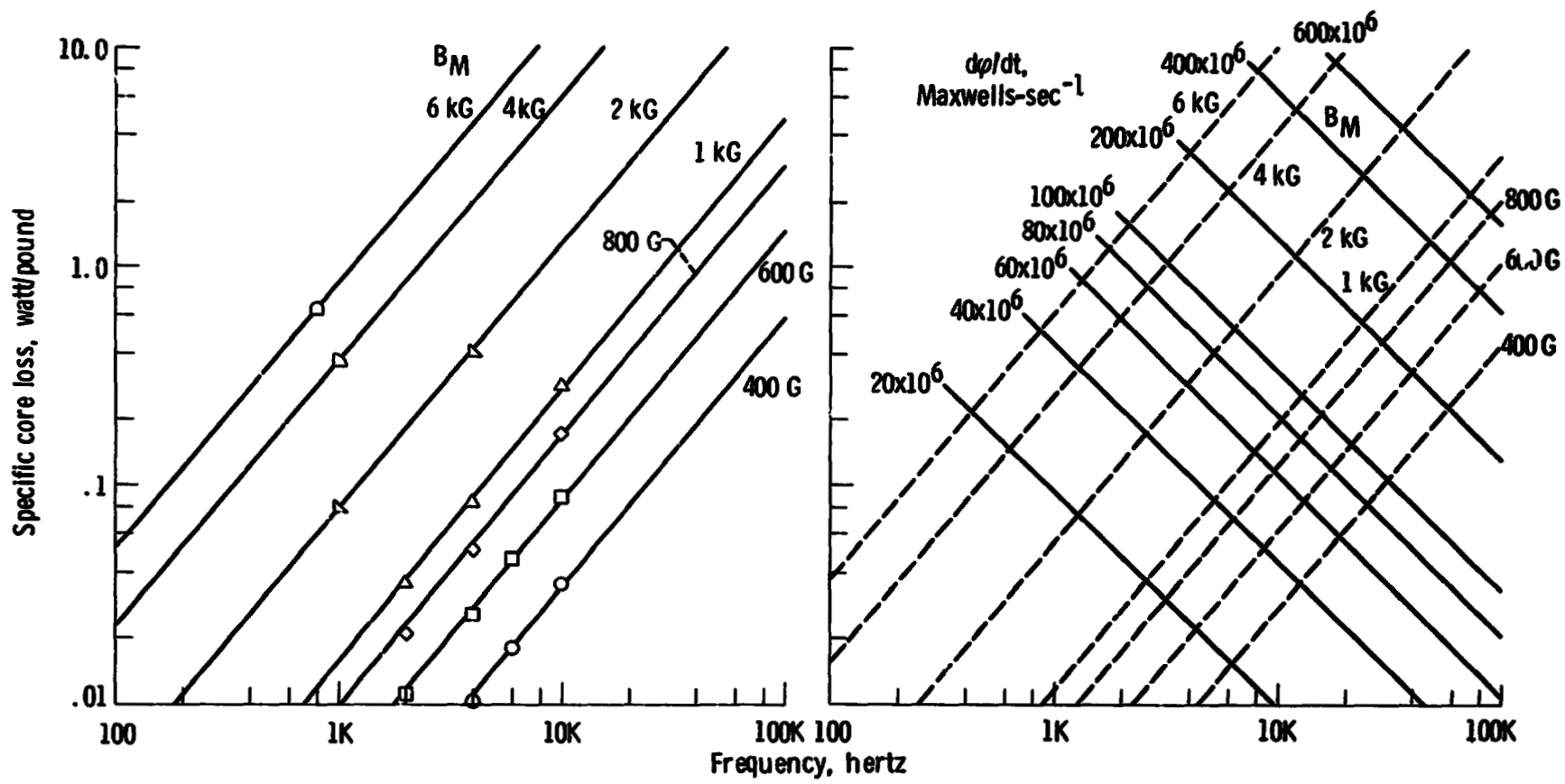


Figure 7. - SCL characteristics for sinusoidal and square wave excitation with axes interchanged.

plotted on the same SCL characteristic (Fig. 7(b)).

3.3 Separation of Loss Variables at Constant Frequency

If excitation is restricted to that of a constant frequency pulse width modulated square wave, the $d\phi/dt$ effects may be determined for various constant values of B_M . Figure 8 shows the instantaneous waveforms for $p(t)$, $i(t)$, and $e(t)$. Positive $i(t)$ values correspond to $H (Ni(t)L^{-1})$ values to the left of the B-axis while negative $i(t)$ values correspond to H values on the right of the B-axis. Also, $p(t)$ values are both positive and negative which corresponds to energy supplied to or energy returned from the core.

Figure 9 shows the instantaneous B-H loop of 1/2 mil Superalloy measured for various $d\phi/dt$ (change in duty cycle) values while holding B_M constant at 6.76 K gauss, and frequency constant at 2 kHz. From this figure, it may be seen that as $d\phi/dt$ increases the B-H loop area for that portion of the cycle also increases. Since the B-H area is proportional to the energy loss, and the additional B-H area is proportional to $d\phi/dt$, it is assumed that the additional half cycle energy loss observed is proportional to $d\phi/dt$.

This procedure was then repeated for several values of B_M with frequency held constant with the results shown in Figure 10. From this figure it is seen that for constant $d\phi/dt$, the total core loss increases with B_M . If the lines of constant B_M could be linearly extrapolated, the ordinate ($d\phi/dt = 0$) intercept would indicate the hysteresis increase with B_M . The eddy current loss is dependent upon both $d\phi/dt$ and B_M . However, it is interesting to note that for a constant value of B_M , the half cycle loss is linearly dependent on

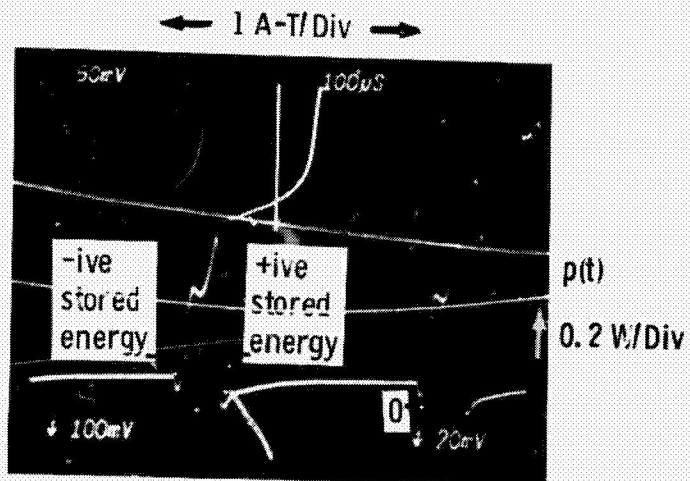
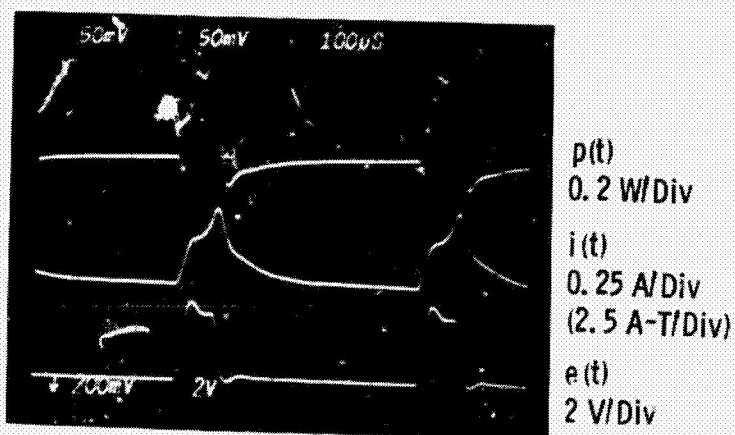
(a) B-H loop and instantaneous $p(t)$.(b) Instantaneous $p(t)$, $i(t)$, and $e(t)$.

Figure 8. - Comparison of the four loss regions for the instantaneous B-H loop, $p(t)$, $i(t)$, and $e(t)$.

ORIGINAL PAGE IS
OF POOR QUALITY

ORIGINAL PAGE IS
OF POOR
QUALITY

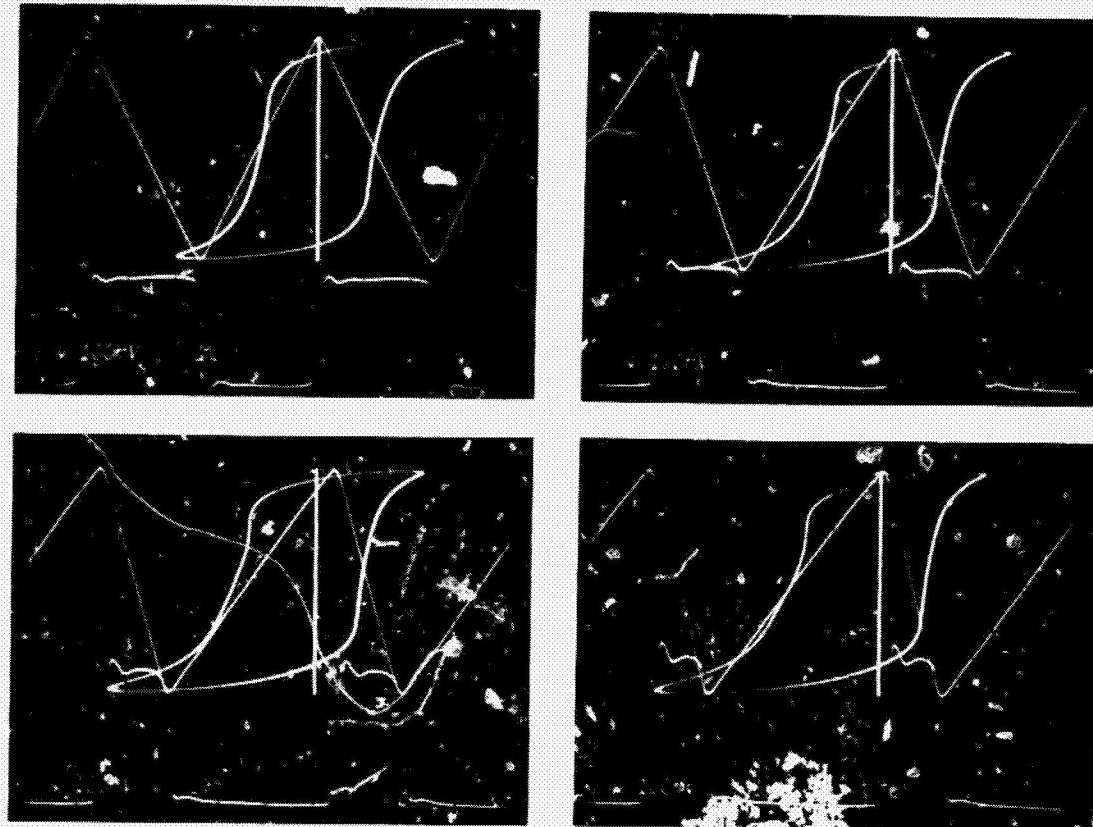


Figure 9. B-H loop as a function of $d\phi/dt$ for constant B_m and f .

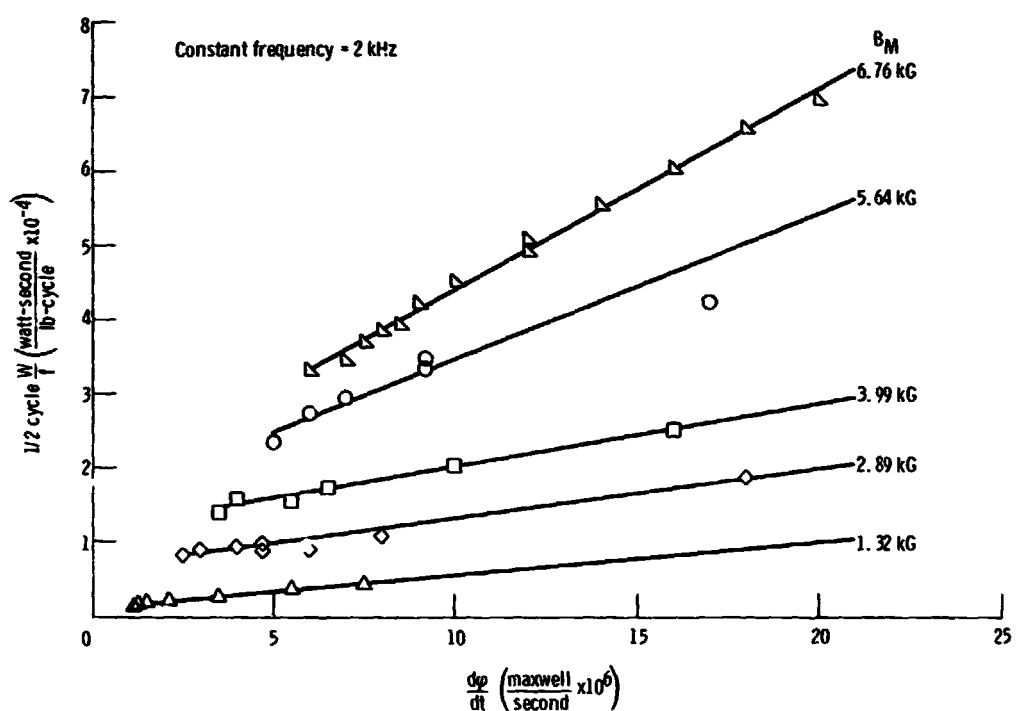
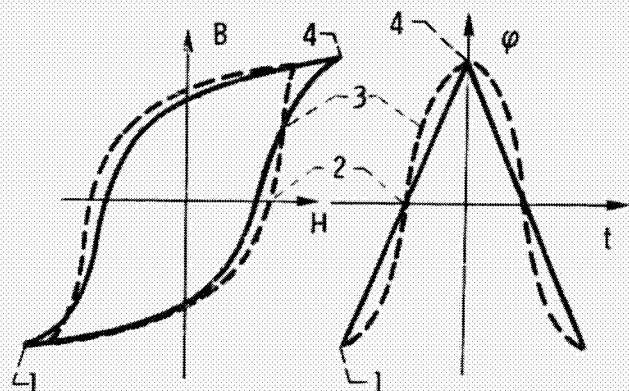
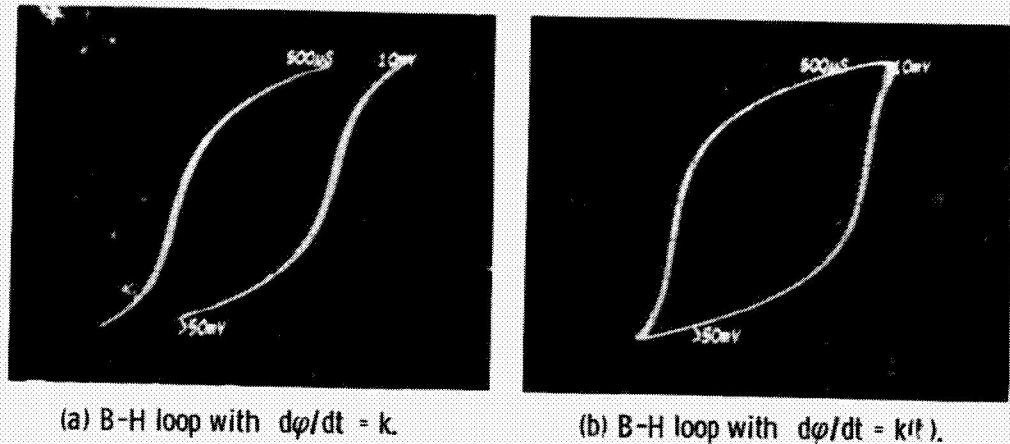


Figure 10. - Half cycle specific core loss per cycle vs. $\frac{dp}{dt}$ with B_M as a parameter.

$d\phi/dt$. This procedure shows that a true separation of the variables $d\phi/dt$, and B_M may be achieved using pulse width modulated square wave excitation techniques. These characteristics will be used to qualitatively explain the differences observed in the B-H loop for sinusoidal and square wave excitation.

A comparison of the B-H loop characteristics under both constant (square wave (fig. 11(a)) and variable (sinusoidal (fig. 11(b))) $d\phi/dt$ conditions measured while holding both frequency and B_M (relates to hysteresis loss) constant is shown in Figure 11. Figure 11(c) illustrates some interesting conditions which, to the author's knowledge, have never been shown in the literature. It has been shown (Fig. 10) that the total half cycle core loss is composed of a hysteresis loss which is proportional to B_M , and an induced eddy current loss proportional to both $d\phi/dt$ and B_M .

Since B_M is held constant, hysteresis loss is constant, and eddy current loss is dependent on $d\phi/dt$ only. The following qualitative observations may be made. At point 1, $d\phi/dt$ for the sine wave is equal to zero while $d\phi/dt$ for the square wave is equal to some positive constant value greater than zero. Therefore, the core loss for the square wave is greater (wider B-H width) than that for the sine wave at point 1. As the flux density increases to point 2, $d\phi/dt$ for the sine wave reaches its maximum value. This value of $d\phi/dt$ is greater than the $d\phi/dt$ for the square wave, and the corresponding core loss (B-H width) is greater. As the flux density increases to point 3, $d\phi/dt$'s for the sine and square wave are approximately equal. This corresponds to an equal B-H width. As the flux approaches point 4 the same conditions as point 1 are repeated.



(c) Superimposed B-H loops and flux excitations
for constant and variable $d\varphi/dt$ conditions.

Figure 11. - Comparison of B-H loop characteristics for constant and variable $d\varphi/dt$ conditions with frequency and B_m as a constant.

ORIGINAL PAGE IS
OF POOR QUALITY

3.4 Analytical Calculation Methods

Using the SCL characteristics for square wave excitation three methods were developed which analytically predict the SCL of a magnetic material for pulse width modulated square wave excitation. These methods are discussed in detail below.

Method 1 - Specific core loss based on B_M of the core. - The SCL characteristics presented in Figure 7(b) relate the total specific loss (hysteresis + eddy current = total loss) to frequency with B_M as a parameter. This data will be used to determine the core loss characteristics with pulse width modulated square wave core excitation. This method is the most indirect approach to calculating the specific core loss. It requires an accurate measure of the effective cross sectional area of the core. Generally, this is a parameter which is not accurately known by the power electronics designer.

Figure 11 shows the oscilloscope traces of a 1000 Hz square wave operating over a duty cycle range of 10 to 50 percent. For each duty cycle the voltage for the positive cycle is adjusted to a maximum value of 4 volts. The DC offset in the core is held to a minimum. Therefore, the negative and positive half cycle volt-seconds are equal.

In order to use the Figure 7(b) characteristics the B_M value for each duty cycle condition must be determined. This value may be obtained as follows:

3.4 Analytical Calculation Methods

Using the SCL characteristics for square wave excitation three methods were developed which analytically predict the SCL of a magnetic material for pulse width modulated square wave excitation. These methods are discussed in detail below.

Method 1 - Specific core loss based on B_M of the core. - The SCL characteristics presented in Figure 7(b) relate the total specific loss (hysteresis + eddy current = total loss) to frequency with B_M as a parameter. This data will be used to determine the core loss characteristics with pulse width modulated square wave core excitation. This method is the most indirect approach to calculating the specific core loss. It requires an accurate measure of the effective cross sectional area of the core. Generally, this is a parameter which is not accurately known by the power electronics designer.

Figure 1 shows the oscilloscope traces of a 1000 Hz square wave operating over a duty cycle range of 10 to 50 percent. For each duty cycle the voltage for the positive cycle is adjusted to a maximum value of 4 volts. The DC offset in the core is held to a minimum. Therefore, the negative and positive half cycle volt-seconds are equal.

In order to use the Figure 7(b) characteristics the B_M value for each duty cycle condition must be determined. This value may be obtained as follows:

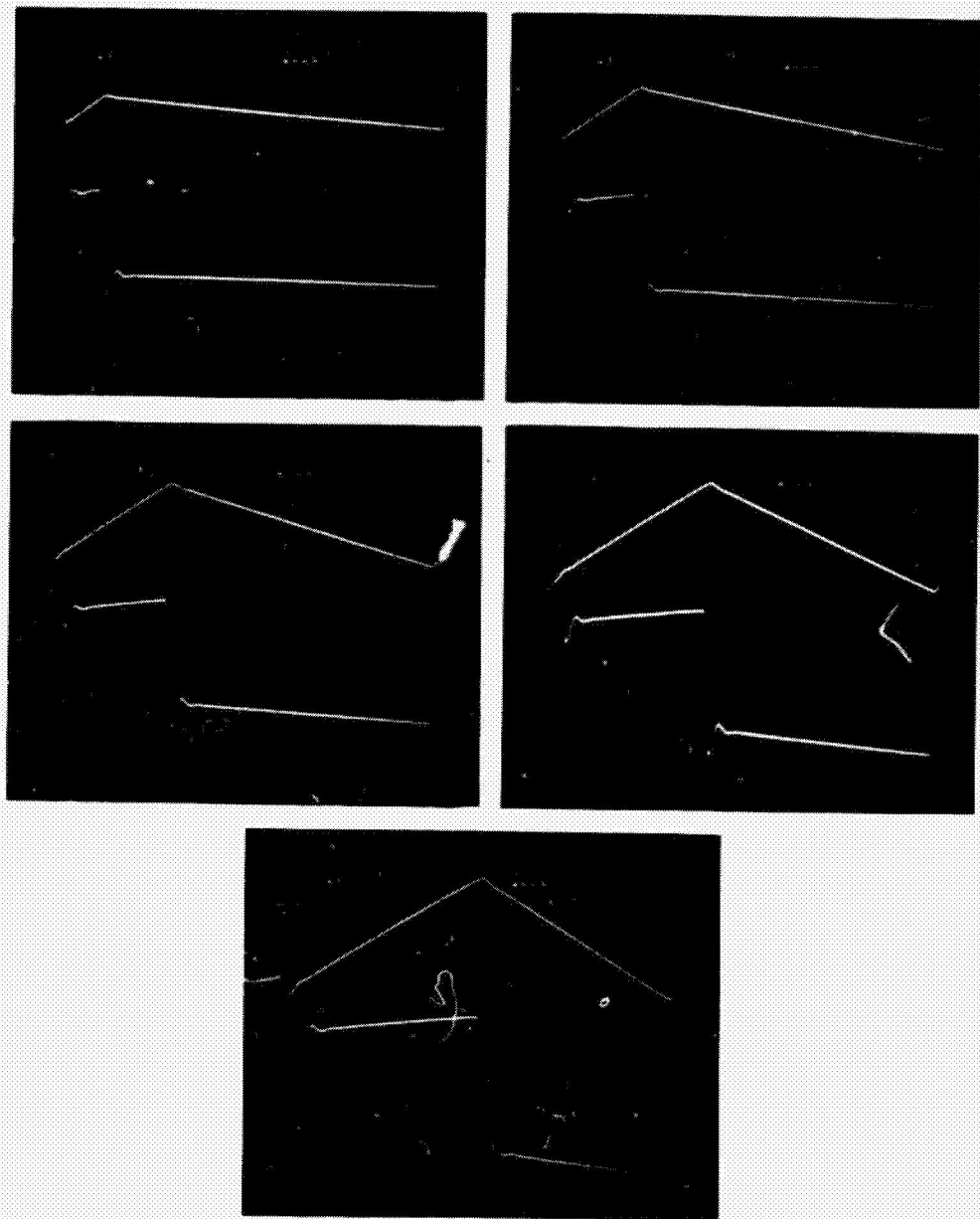


Figure 12. - Waveform excitation for a pulse width modulated square wave.

ORIGINAL PAGE IS
OF POOR QUALITY

From Faraday's law

$$e_c = -N \frac{d\phi}{dt} \times 10^{-8} \text{ (volts)} \quad (3.3)$$

Therefore

$$\frac{d\phi}{dt} = -e_c N^{-1} \times 10^8 \text{ (maxwells/second)} \quad (3.4)$$

For each cycle portion

$$\Delta\phi = (\frac{d\phi}{dt})\Delta t \quad (3.5)$$

$$\Delta\phi = -e_c N^{-1} \Delta t \times 10^8 \quad (3.6)$$

and,

$$B_M = \frac{\Delta\phi}{(2A_e)^{-1}} = -0.5 e_c \Delta t (NA_e)^{-1} \times 10^8 \text{ (gauss)} \quad (3.7)$$

where:

$$A_e = A_c \times SF \text{ (cm}^2\text{)}$$

N = number of turns

e_c , Δt → related to duty cycle

Using 1/2 mil Supermalloy as an example, for a frequency of 1000 Hz, the B_M values corresponding to each duty cycle width can be determined as follows:

$$\begin{aligned} B_M \text{ (positive cycle)} &= -0.5 (3.9) (100 \times 10^{-6}) (10 \times 1.97)^{-1} \times 10^8 \\ &= -990 \text{ gauss} \end{aligned}$$

$$\begin{aligned} B_M \text{ (negative cycle)} &= -0.5 (-0.44) (900 \times 10^{-6}) (10 \times 1.97)^{-1} \times 10^8 \\ &= 1000 \text{ gauss} \end{aligned}$$

$$B_M \text{ (positive cycle)} \approx B_M \text{ (negative cycle)}$$

Considering the positive half cycle only this calculation can be repeated for the remaining four cases with the results shown below:

Duty cycle, percent	$\Delta t-\mu s$	e_c^+ , volts	B_M^+ , gauss
10	100	3.9	990
20	200	3.9	1980
30	300	3.9	2470
40	400	3.8	3858
50	500	3.4	4315

This data can now be used with Figure 7(b) to determine the specific core loss associated with each duty cycle condition. The results of these calculations are shown on Figure 13.

During the experiment the specific core loss was measured for each duty-cycle condition. A comparison between the measured and calculated results is shown in Figure 14. At the 50 percent duty-cycle condition the error between the measured and calculated specific core loss was:

$$SCL_{calc} = 0.31 \text{ W/lb}$$

$$SCL_{meas} = 0.339 \text{ W/lb}$$

$$\text{percent error} = \frac{SCL_{meas} - SCL_{calc}}{SCL_{meas}} \times 100 \quad (3.8)$$

$$\text{percent error} = \frac{0.339 - 0.31}{0.339} \times 100 = 8.6 \text{ percent}$$

From these results it may be seen that the specific core loss can be easily calculated for pulse width modulated square waves if the base frequency, excitation voltage level, duty-cycle, number of turns, and the effective cross sectional area of the core is known. Also, for a constant input voltage as the duty cycle increases, B_M increases, and the specific core loss of the magnetic device increases.

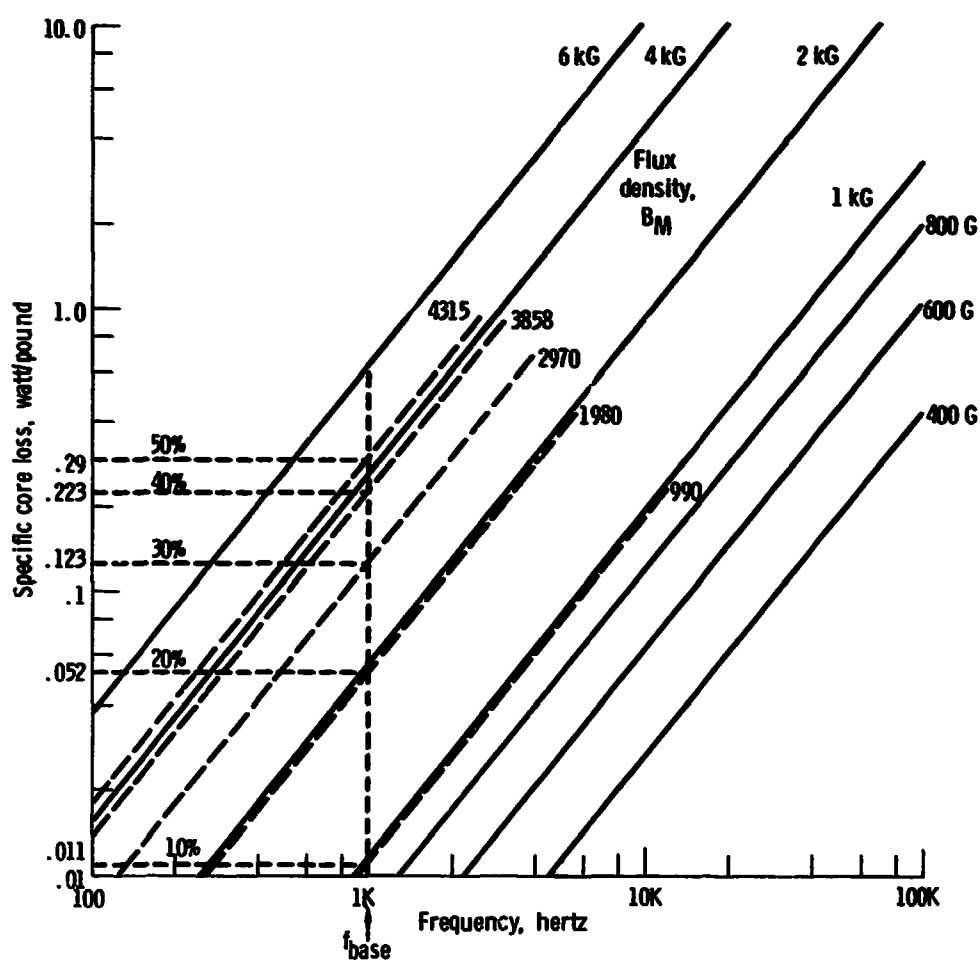


Figure 13. - Specific core loss characteristics for cut 1/2 mil Supermalloy under duty cycle conditions.

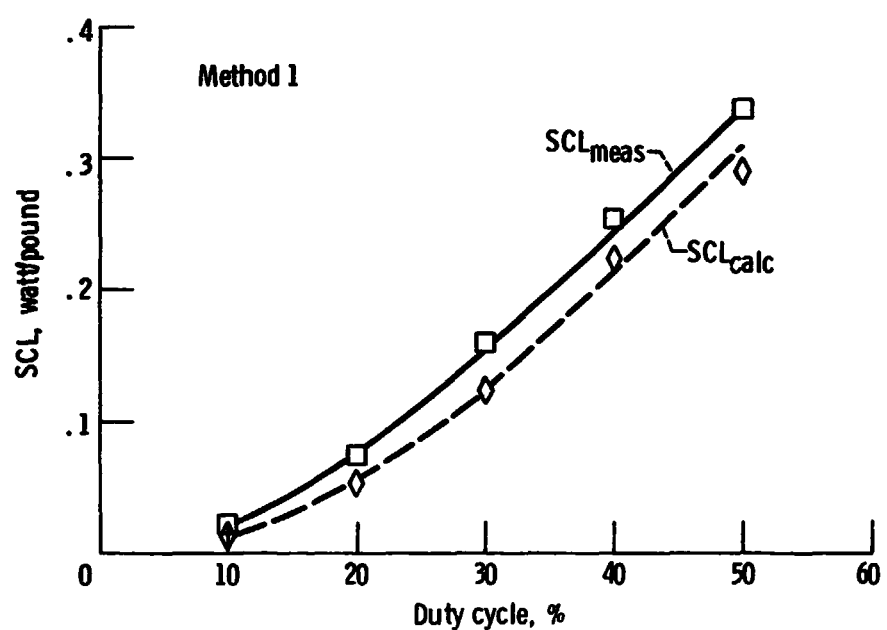


Figure 14. - Comparison of calculated vs measured values of SCL for 1/2 mil Supermalloy as a function of duty cycle for a 1 kHz - 3.9 volt pulse voltage.

Method 2 - Specific core loss based on $d\phi/dt$ in the core. - The specific core loss characteristics presented in Figure 7(b) relate the total specific core loss to frequency with B_M and $d\phi/dt$ as parameters. If the B_M parameter is ignored on this figure, the specific core loss can be calculated by using the $d\phi/dt$ parameter and an equivalent excitation frequency.

In the discussion of Section 3.3 the core loss was shown to be a function of B_M and $d\phi/dt$. For a pulse width modulated square wave with a constant positive $d\phi/dt$ and constant negative $d\phi/dt$, B_M is determined directly by the length of time that the pulse is on. The width of this "on pulse" has an "equivalent" frequency of

$$f_{eq} = T_{eq}^{-1} = (2t_{on})^{-1} \quad (3.9)$$

Also, it was shown that the total specific core loss per cycle could be broken down into a half cycle loss dependent on $d\phi/dt$. Therefore, the total specific core loss may be determined using the following relationship.

$$\text{Total SCL} = (\text{SCL/cycle}) (\text{excitation frequency})$$

$$= \left(\frac{1}{2} \frac{\text{SCL}^+}{f_{eq}^+} + \frac{1}{2} \frac{\text{SCL}^-}{f_{eq}^-} \right) f_{ex} \quad (3.10)$$

where

SCL^+ positive cycle specific core loss

SCL^- negative cycle specific core loss

f_{eq}^+ positive cycle equivalent frequency

f_{eq}^- negative cycle equivalent frequency

f_{ex} excitation frequency

Example:

10 percent duty-cycle case:

$$e_c^+ = 3.9 \text{ V}$$

$$e_c^- = 0.44 \text{ V}$$

$$f_{ex} = 1000 \text{ Hz}$$

$$t_{on}^+ = 100 \times 10^{-6} \text{ sec}$$

$$t_{on}^- = 900 \times 10^{-6} \text{ sec}$$

Then

$$f_{eq}^+ = (2t_{on}^+)^{-1} = (2 \times 100 \times 10^{-6})^{-1} = 5 \text{ kHz}$$

$$f_{eq}^- = (2t_{on}^-)^{-1} = (2 \times 900 \times 10^{-6})^{-1} = 555 \text{ Hz}$$

using Faraday's law

$$d\phi/dt = e_c N^{-1} \times 10^8$$

$$(d\phi/dt)^+ = 3.9(10)^{-1} \times 10^8 = 39 \times 10^6 \text{ maxwells/sec}$$

$$(d\phi/dt)^- = 0.44(10)^{-1} \times 10^8 = 4.4 \times 10^6 \text{ maxwells/sec}$$

Replotting Figure 7(b) as Figure 15 with $(d\phi/dt)^+$, $(d\phi/dt)^-$, f^+ , and f^- shown, the corresponding SCL's may be read directly from the figure:

$$SCL^+ = 0.082 \text{ watt/pound}$$

$$SCL^- = 0.0063 \text{ watt/pound}$$

Using the equation for the total SCL the following results are obtained:

$$\text{Total SCL} = \frac{1}{2} \left(\frac{0.082}{5000} + \frac{0.0063}{555} \right) 1000$$

$$\text{Total SCL} = 0.014 \text{ watt/pound}$$

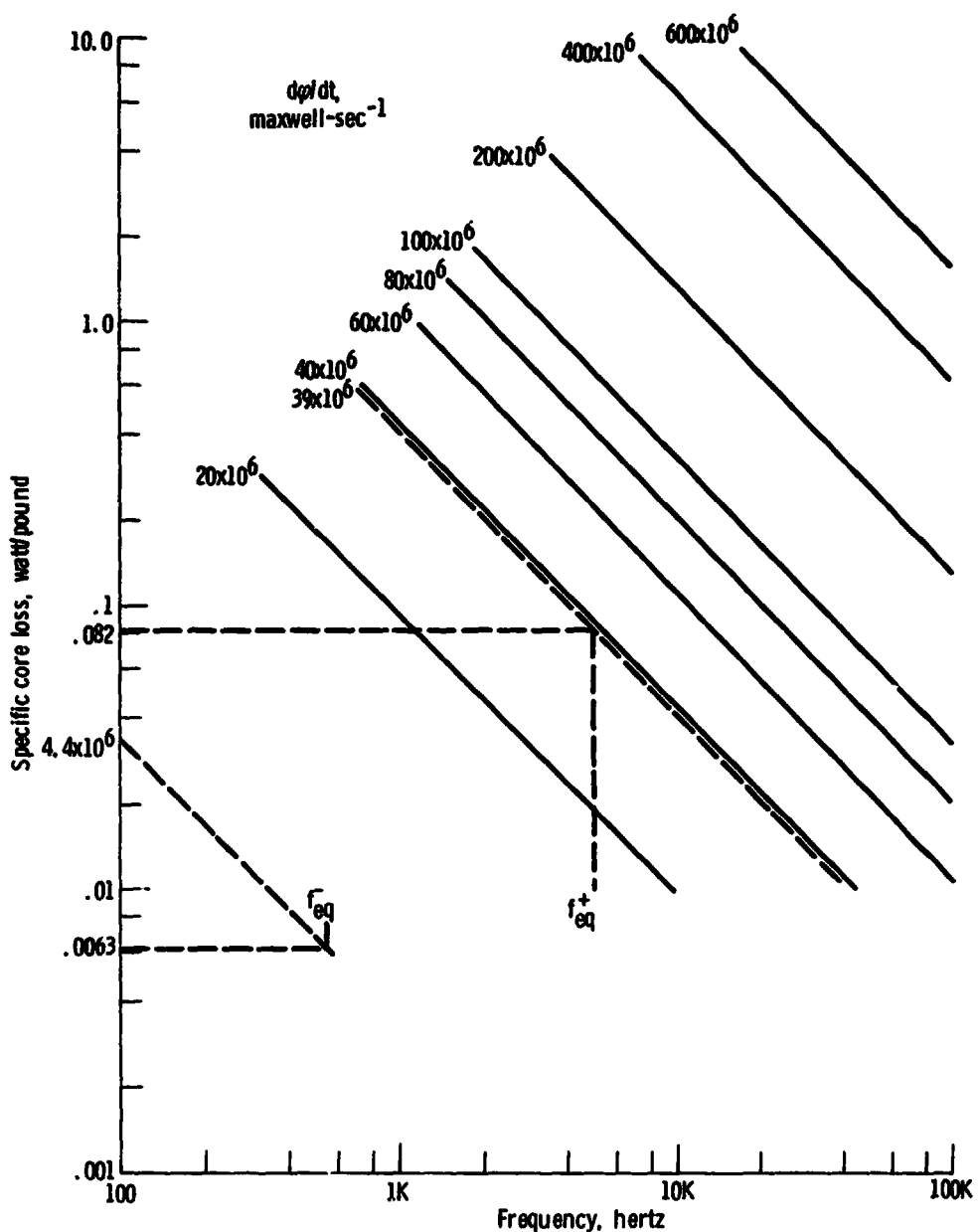


Figure 15. - SCL for f_{eq}^+ and f_{eq}^- with an excitation frequency (f_{ex}) of 1 kHz and 10% duty cycle.

summarizing the results for the other conditions we have:

$$f_{base} = 1000 \text{ Hz}$$

Duty cycle, percent	f_{eq}^+ , Hz	f_{eq}^- , Hz	$\frac{d\phi^+}{dt} \times 10^6$ max/sec	$\frac{d\phi^-}{dt} \times 10^6$ max/sec
10	5000	555	39	4.4
20	2500	625	39	10
30	1670	714	39	16
40	1250	833	38	26
50	1000	1000	34	34

From Figure 15 the SCL^+ and SCL^- can be obtained. Again using the total SCL equation:

20 percent duty cycle:

$$\text{Total SCL} = \frac{1}{2} \left(\frac{0.162}{2500} + \frac{0.0275}{625} \right) 1000 = 0.054 \text{ W/lb}$$

30 percent duty cycle:

$$\text{Total SCL} = \frac{1}{2} \left(\frac{0.24}{1670} + \frac{0.074}{714} \right) 1000 = 0.124 \text{ W/lb}$$

40 percent duty cycle:

$$\text{Total SCL} = \frac{1}{2} \left(\frac{0.3}{1250} + \frac{0.192}{833} \right) 1000 = 0.235 \text{ W/lb}$$

50 percent duty cycle:

$$\text{Total SCL} = \frac{1}{2} \left(\frac{0.3}{1000} + \frac{0.3}{1000} \right) 1000 = 0.3 \text{ W/lb}$$

In Figure 16 these calculated SCL's are compared with the measured SCL values for these duty-cycle conditions. The percent error is the same as obtained with method 1 (8.6 percent).

Method 3 - Specific core loss based on incremental $d\phi/dt$ in the core. - The technique developed in method 2 allows determination of the specific core loss based on the $d\phi/dt$ value for the entire positive or the entire negative cycle of the square wave. In Sec-

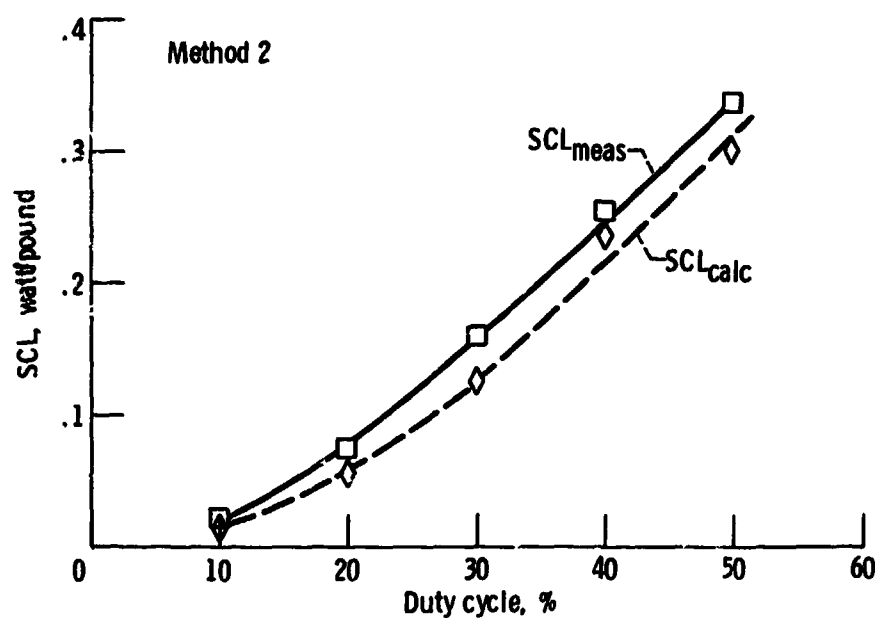


Figure 16. - Comparison of calculated vs measured values of SCL as a function of duty-cycle for a 1 kHz - 3.9 volt pulse voltage.

tion 3.3 the dependency of the B-H width on $d\phi/dt$ was developed. For a particular frequency and B_M level a family of curves could be developed for various $d\phi/dt$ values as shown in Figure 17. Using actual square waves observed in this experiment (Fig. 12), it can be seen that for any interval the actual exciting voltage is not a constant value. This would indicate that the corresponding $d\phi/dt$ values over the cycle are not of constant value. If the waveform is broken down into discrete sample intervals the corresponding locus of points on the B-H loop may be plotted as Δt is incremented. The corresponding B-H width would be a direct function of the pulse height for that interval. Figure 17(b) shows how the pulse height, $d\phi/dt$, and Δt would translate into a locus of points on the B-H loop. This approach may be used to explain the B-H loop shapes observed under various excitation conditions.

Relating these various $d\phi/dt$ rates to loss at the positive equivalent frequency, the SCL characteristics of Figure 17(c) may be used to determine the incremental core loss.

The loss per interval is calculated as follows:

$$T^+ = n \Delta t_i^+ = \frac{1}{2f^+} \quad (3.11)$$

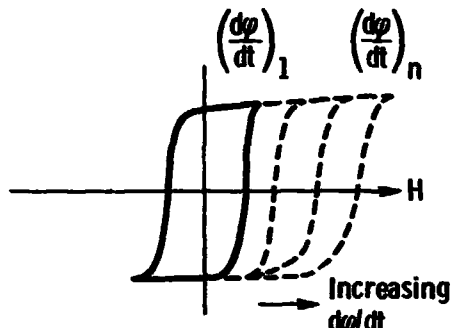
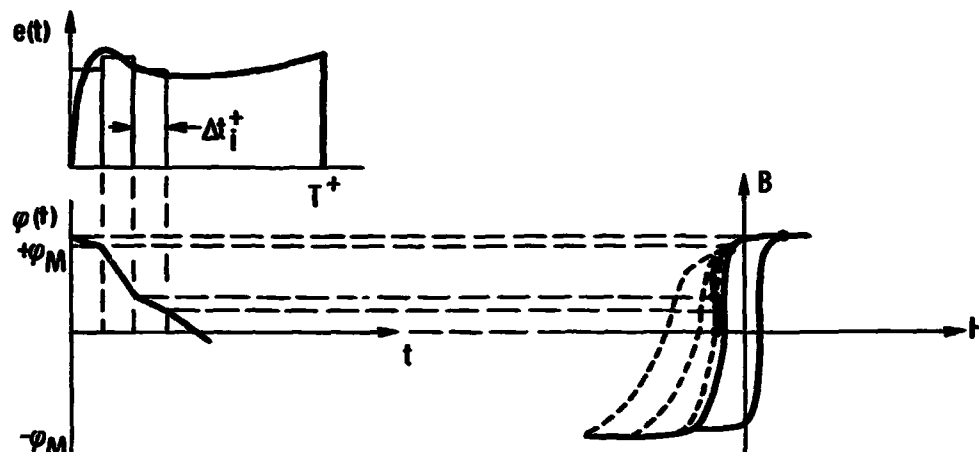
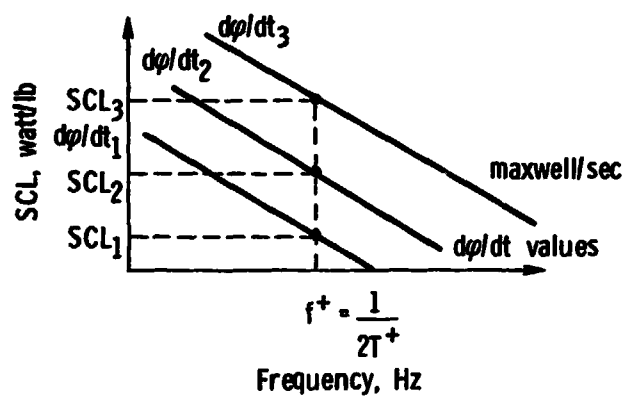
where n = number of increments

$$\Delta t_i^+ = \frac{1}{2nf^+} \quad (3.12)$$

The energy dissipated in Δt_i^+ would be:

$$\Delta E_i^+ = SCL_i^+ \Delta t_i^+ = \frac{SCL_i^+}{2nf^+} \quad (3.13)$$

If Δt_i^+ were made small enough, the difference between the incre-

(a) Family of curves for various $d\phi/dt$ values.(b) Relationship of incremental $d\phi/dt$ rates to B-H loop.(c) SCL characteristics for various $d\phi/dt$ values.Figure 17. - Family of B-H loops and SCL characteristics based on $d\phi/dt$ as a parameter.

mental excitation and the actual excitation would approach zero as a limit.

The total energy over the positive cycle is simply the summation of the incremental ΔE^+ 's:

$$E_T^+ = \sum_{i=1}^N \Delta E_i^+ = \frac{1}{2nf^+} \sum_{i=1}^n SCL_i^+ \quad \frac{\text{W-sec}}{\text{lb-cycle}} \quad (3.14)$$

Similarly the total energy for the negative cycle is

$$E_T^- = \sum_{i=1}^M \Delta E_i^- = \frac{1}{2mf^-} \sum_{i=1}^m SCL_i^- \quad \frac{\text{W-sec}}{\text{lb-cycle}} \quad (3.15)$$

and the average power would be:

$$SCL_T = \text{specific power loss} = \frac{E_T^+ + E_T^-}{T^+ + T^-} \quad \text{W/lb} \quad (3.16)$$

Applying this technique to the 10 percent PWM square wave case we have:

Positive cycle			
Interval ($\Delta t_i = 20 \mu\text{s}$)	e_c , volts	$\frac{d\phi}{dt} \div 10^6$ max/sec	SCL_i^+ , W/lb
1	3.4	34	0.063
2	4.0	40	.092
3	3.9	39	.087
4	3.9	39	.087
5	4.0	40	<u>.092</u>
			$\Sigma 0.421$

Negative cycle

Interval ($\Delta t_i = 100 \mu s$)	e_c , volts	$\frac{d\phi}{dt} : 10^6$ max/sec	SCL_i^- , W/lb
1	0.2	2	0.00092
2	.4	4	.0044
3	.4	4	.0044
4	.4	4	.0044
5	.44	4.4	.0055
6	.5	5	.0074
7	.5	5	.0074
8	.55	5.5	.0091
9	.55	5.5	<u>.0091</u>
Σ			0.05262

$$E_T^+ = \frac{1}{2 \times 5 \times 5000} (0.421) = 8.42 \times 10^{-6} \frac{\text{W-sec}}{\text{lb-cycle}}$$

$$E_T^- = \frac{1}{2 \times 9 \times 555} (0.05262) = 5.267 \times 10^{-6} \frac{\text{W-sec}}{\text{lb-cycle}}$$

$$SCL_T = \frac{8.42 \times 10^{-6} + 5.267 \times 10^{-6}}{100 \times 10^{-6} + 900 \times 10^{-6}} = 0.014 \text{ W/lb}$$

For the remaining cases we have

20 percent:

$$\sum_{i=1}^{10} SCL_i^+ = 1.764 \quad \Delta t_i^+ = 20 \mu s$$

$$\sum_{i=1}^8 SCL_i^- = 0.298 \quad \Delta t_i^- = 100 \mu s$$

$$SCL_T = \frac{\frac{1.764}{2 \times 10 \times 2500} + \frac{0.298}{2 \times 8 \times 625}}{200 \times 10^{-6} + 800 \times 10^{-6}} = 0.065 \text{ W/lb}$$

30 percent:

$$\sum_{i=1}^{15} SCL_i^+ = 4.554 \quad \Delta t_i^+ = 20 \text{ } \mu\text{s}$$

$$\sum_{i=1}^7 SCL_i^- = 0.621 \quad \Delta t_i^- = 100 \text{ } \mu\text{s}$$

$$SCL_T = \frac{\frac{4.554}{2 \times 15 \times 1670} + \frac{0.621}{2 \times 7 \times 714}}{300 \times 10^{-6} + 700 \times 10^{-6}} = 0.153 \text{ W/lb}$$

40 percent:

$$\sum_{i=1}^{20} SCL_i^+ = 8.204 \quad \Delta t_i^+ = 20 \text{ } \mu\text{s}$$

$$\sum_{i=1}^6 SCL_i^- = 1.117 \quad \Delta t_i^- = 100 \text{ } \mu\text{s}$$

$$SCL_T = \frac{\frac{7.73}{2 \times 20 \times 1250} + \frac{1.117}{2 \times 6 \times 833}}{400 \times 10^{-6} + 600 \times 10^{-6}} = 0.266 \text{ W/lb}$$

50 percent:

$$\sum_{i=1}^{25} SCL_i^+ = 9.03 \quad \Delta t_i^+ = 20 \text{ } \mu\text{s}$$

$$\sum_{i=1}^5 SCL_i^- = 1.66 \quad \Delta t_i^- = 100 \text{ } \mu\text{s}$$

$$SCL_T = \frac{\frac{9.03}{2 \times 25 \times 1000} + \frac{1.66}{2 \times 5 \times 1000}}{500 \times 10^{-6} + 500 \times 10^{-6}} = 0.347 \text{ W/lb}$$

A comparison of this value with the measured results is shown in

Figure 18. The error using this technique is less than that of methods 1 and 2.

The instantaneous $p(t)$ waveforms are shown in figure 19. A Phillips PM3252 multiplying oscilloscope was used to obtain $p(t)$. In the top photo a resistive load was used to verify the accuracy of the multiplier. For the square wave the growth of $p(t)$ is fairly linear with time, which supports the preliminary assumptions used in developing this method.

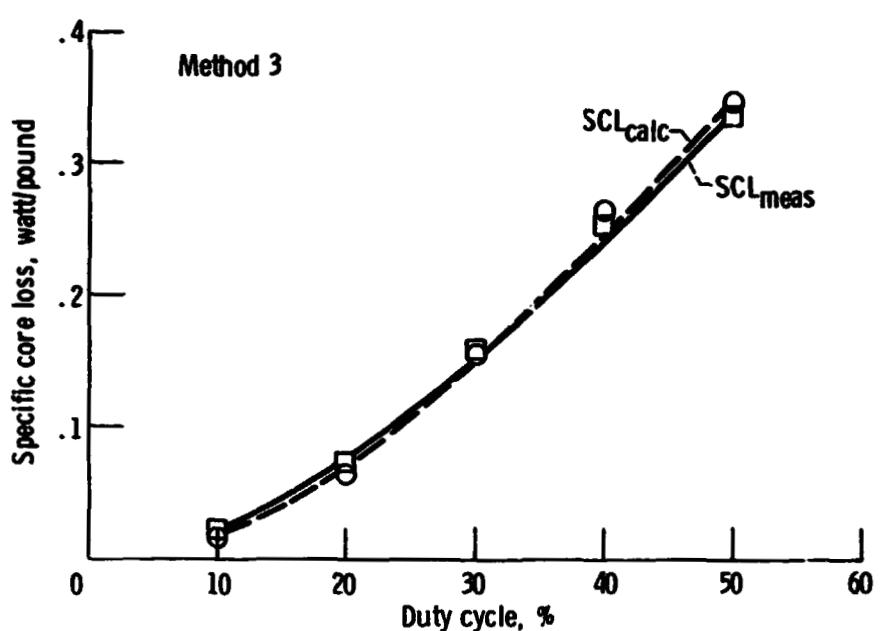


Figure 18. - Comparison of calculated vs measured values of SCL as a function of duty cycle for a 1 kHz - 3.9 volt pulse voltage.

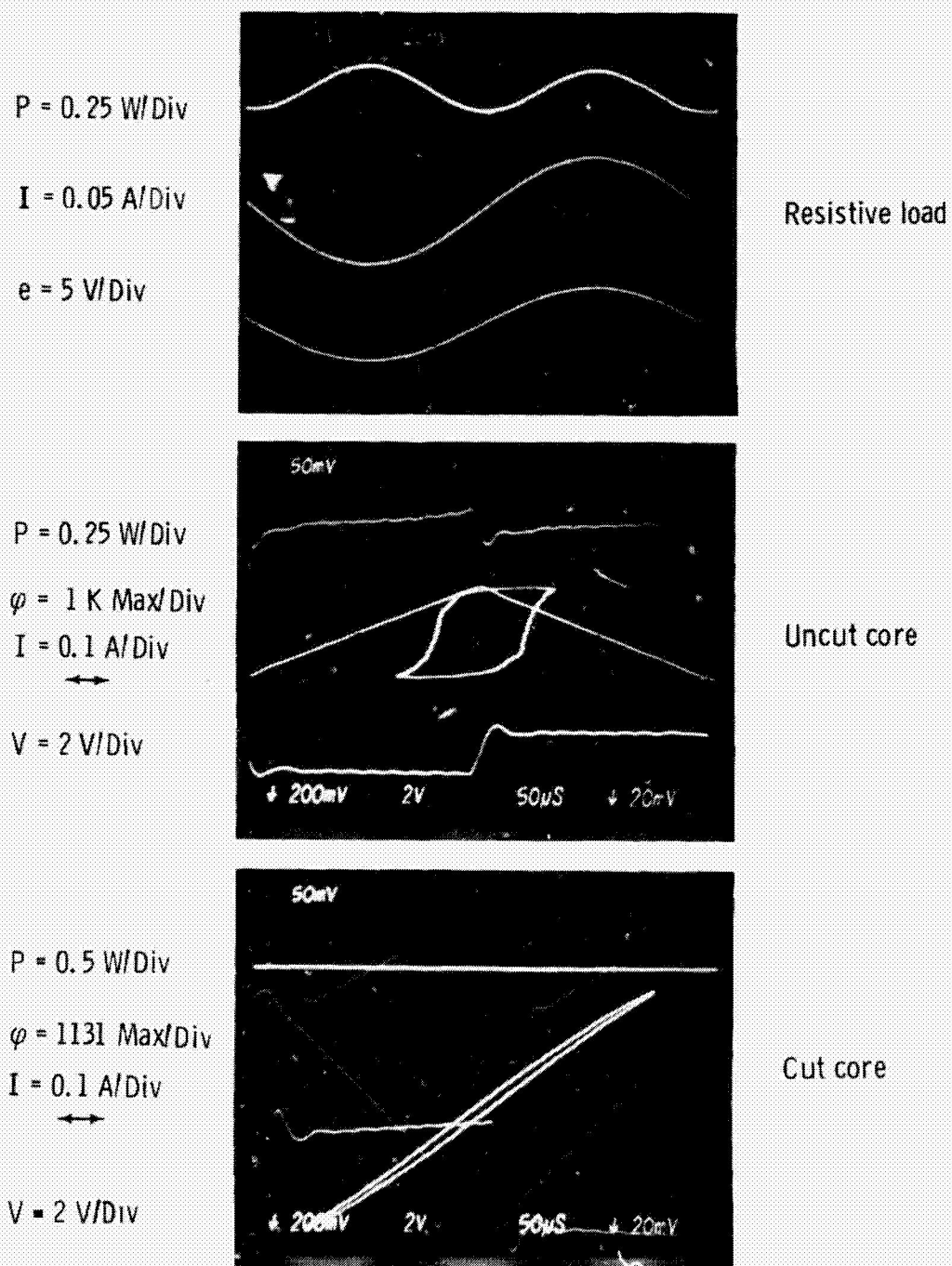


Figure 19. - Instantaneous energy characteristics.

CHAPTER IV
GENERAL CORE LOSS ANALYSIS

4.1 Introduction

Analysis techniques such as harmonic analysis and digital simulation of eddy current losses have previously been used for prediction of core losses of distorted flux waveforms (Ref. 24). Eddy current correction factors (Ref. 25) have also been employed in estimating the core loss of sinusoidal excitation considering only the fundamental and one harmonic component. In this chapter method 3 of the previous chapter is used to analytically predict the specific core loss for several distorted waveform excitations.

Since this method is based upon the summation of a large number of sample points, the digital computer was used for high speed core loss analysis. In order to minimize the number of subroutines of the computer algorithm, a general characteristic equation was derived using experimental data. This equation relates SCL to the equivalent frequency and $d\phi/dt$. An alternate equation which relates SCL to equivalent frequency and B_M was also derived. For analysis of the SCL characteristics a specific magnetic material having a known tape or grain thicknesses, only a constant and two exponent values must be supplied in the initial data format.

Using the square wave SCL characteristics and the computer algorithm, analyses were performed for sinusoidal and nonsinusoidal excitation conditions using Supermalloy, Square Permalloy 80, and ferrite

materials. As a final illustration of the method, the sinusoidal core loss characteristics of a 1/2 mil Supermalloy material operating at 1000 Hz is measured experimentally and calculated analytically.

4.2 Development of Computer Algorithms

The SCL characteristics for various types of magnetic materials is presented in appendix A. Due to the logarithmic nature of the characteristics, the SCL equation for either the $d\phi/dt$ parameter or the B_M parameter would have the following form:

$$SCL = af_{eq}^x \quad (4.1)$$

The exponent x could be either positive (let $x = d$) or negative (let $x = u$) depending upon the parameter being examined. The constant a is also a logarithmic function of either $d\phi/dt$ or B_M . The equation for the constant is as follows:

$$a = g(d\phi/dt)^c \quad (\text{for the } d\phi/dt \text{ parameter}) \quad (4.2)$$

or

$$a = s(B_M)^z \quad (\text{for the } B_M \text{ parameter}) \quad (4.3)$$

Combining Equation (4.1) with the appropriate constant equation, the following two equation forms may be used to determine the SCL for a specific frequency and B_M or $d\phi/dt$ level:

For $d\phi/dt$:

$$SCL = g(d\phi/dt)^c f_{eq}^u \quad (4.4)$$

For B_M :

$$SCL = s(B_M)^z f_{eq}^d \quad (4.5)$$

Values for the constants g and s , and for the exponents c , d , z , and u for various magnetic materials were determined from the

experimental data shown in appendix A. These calculated values are shown in tables II and III. In Equation (4.5) at low flux densities, the d exponent was determined by Steinmetz to be 1.6 for electrical sheet steel (Ref. 26). For higher flux densities the value of the exponent may be as high as 2.5. The values of the exponent as measured in these experiments falls within this upper limit. The value of the exponent was found to be dependent upon both the magnetic material and the tape thickness.

TABLE II. - TABULATION OF THE CONSTANT AND EXPONENT
VALUES USED IN EQUATION (4.4)

Table II.1. - Supermalloy-Cut Core

Constant	Tape thickness, mils			
	0.5	1.0	2.0	4.0
c	2.270	1.563	1.981	1.959
g	2.537×10^{-15}	3.819×10^{-10}	3.240×10^{-15}	4.420×10^{-14}
u	-1.000	-0.811	-0.500	-0.345

Table II.2. - Supermalloy - Uncut

Constant	Tape thickness, mils			
	0.5	1.0	2.0	4.0
c	1.951	2.000	2.090	2.040
g	7.48×10^{-13}	4.430×10^{-13}	3.259×10^{-15}	1.124×10^{-14}
u	-0.408	-0.825	-0.561	-0.297

Table II.3. - Square Permalloy 80 - Uncut

Constant	Tape thickness, mils			
	0.5	1.0	2.0	4.0
c	0.985	1.713	1.704	1.739
g	-1.845×10^{-6}	2.759×10^{-12}	1.201×10^{-12}	9.202×10^{-13}
u	-0.349	-0.225	-0.226	-0.258

Table II.4. - Ferrite

Constant	Material
	3B7
c	2.64
g	1.544×10^{-15}
u	-1.6

TABLE III. - TABULATION OF THE CONSTANT AND EXPONENT

VALUES USED IN EQUATION (4.5)

Table III.1. - Supermalloy - Cut Core

Constant	Tape thickness, mils			
	0.5	1.0	2.0	4.0
d	1.210	1.307	1.467	1.670
z	2.038	2.084	1.948	1.948
s	2.876×10^{-12}	1.065×10^{-12}	7.99×10^{-13}	3.231×10^{-13}

Table III.2. - Supermalloy - Uncut

Constant	Tape thickness, mils			
	0.5	1.0	2.0	4.0
d	1.230	1.300	1.53	1.750
z	1.940	2.000	2.110	2.020
s	4.297×10^{-12}	8.676×10^{-13}	9.578×10^{-14}	1.056×10^{-13}

Table III.3. - Square Permalloy 80 - Uncut

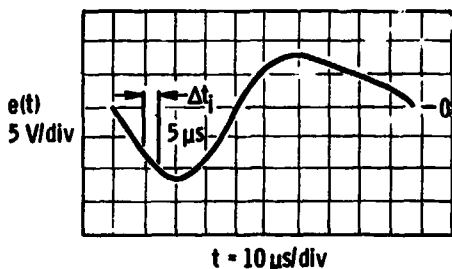
Constant	Tape thickness, mils			
	0.5	1.0	2.0	4.0
d	0.624	1.456	1.459	1.613
z	.976	1.696	1.722	1.884
s	1.718×10^{-6}	7.054×10^{-12}	7.330×10^{-12}	9.447×10^{-13}

Table III.4. - Ferrite

Constant	Material
	3B7
d	1.04
z	2.67
s	3.024×10^{-13}

The use of Equations (4.4) and (4.5) is not restricted to a computer algorithm. By using a simple hand calculator and the analysis methods described in Section 3.4 the SCL for a particular magnetic material and tape thickness may be easily determined. An example of this process is shown in Figure 20. For the waveform shown the positive half cycle frequency is 8.77 kHz, and the negative half cycle frequency is 12.5 kHz. The measured SCL for this waveshape is 0.144 watts/pound. If the SCL is calculated using 5 μ s intervals, the calculated value is 0.132 watt/pound. This represents an error of 8.3 percent. This error will be reduced by decreasing the sample interval.

A computer algorithm was developed which automates the analysis of the large number of sample points encountered in applying this method. A listing of the program is shown in Figure 21. The input/



Waveform excitation into a 1/2 mil
Supermalloy cut core

$$SCL = 2.537 \times 10^{-15} (\frac{d\phi}{dt})^2 \cdot 27 f_{eq}^{-1} \quad (4.3)$$

	Internal	$e(t) - V$	$\frac{d\phi}{dt} - \text{maxwell/sec}$	SCL watt/lb
-ive half cycle	1	0	0	0
	2	2.5	25×10^6	.013
	3	6.5	65×10^6	.110
	4	9.5	95×10^6	.261
	5	11.5	115×10^6	.403
	6	11.0	110×10^6	.364
	7	8.5	85×10^6	.203
	8	5	5×10^6	0.000
+ive half cycle	1	0	0	0
	2	3	30×10^6	.027
	3	6.5	65×10^6	.157
	4	8.2	82×10^6	.266
	5	8.0	80×10^6	.297
	6	7.0	70×10^6	.186
	7	6.5	65×10^6	.157
	8	5.8	58×10^6	.121
	9	5.0	50×10^6	.087
	10	3.5	35×10^6	.039
	11	3.0	30×10^6	.027
	12	1.0	10×10^6	.002
	13	0	0	0

Using equation 3.16

$$SCL_T = \frac{1.354}{2 \times 8 \times 12.5 \times 10^3} + \frac{1.355}{2 \times 13 \times 8.77 \times 10^3} = 0.132 \text{ watt-pound}$$

$$96.9 \times 10^{-6}$$

Figure 20. - An example to demonstrate the application of method 3 and the specific core loss equations.

```

0000100 DIMENSION V(2,100),DPDT(2,100),SCL(2,100)
0000200 DATA SUPER,SUPERM,SQOPTH,FERV/'S','D','A','F'/
0000300 C NUMBER OF TURNS ON TRANSFORMER PRIMARY
0000400 READ(S,100) T
0000500 C NUMBER OF DATA POINTS FOR + PRIMARY VOLTAGE
0000600 READ(S,110) J
0000700 C NUMBER OF DATA POINTS FOR - PRIMARY VOLTAGE
0000800 READ(S,110) K
0000900 C VALUE OF DATA INCREMENT IN MICROSECONDS
0001000 READ(S,100) TINC
0001100 TJ=J
0001200 TK=K
0001300 FON=1./(2.*TINC*TJ+1.E-6)
0001400 FOFF=1./(2.*TINC*TK+1.E-6)
0001500 C READ IN + PRIMARY VOLTAGE VALUES
0001600 DO 10 I=1,J
0001700 READ(S,100)V(1,I)
0001800 DPDT(1,I)=V(1,I)/(T*1.E-8)
0001900 10 CONTINUE
0002000 C READ IN - PRIMARY VOLTAGE VALUES
0002100 DO 20 I=1,K
0002200 READ(S,100)V(2,I)
0002300 DPDT(2,I)=V(2,I)/(T*1.0E-8)
0002400 20 CONTINUE
0002500 C OUTPUT OF INITIAL DATA ENTRY
0002600 WRITE(6,199)
0002700 WRITE(6,600)
0002800 WRITE(6,200) T
0002900 C OUTPUT + VOLTAGE INFO
0003000 WRITE(6,210)FON
0003100 WRITE(6,230)
0003200 DO 30 I=1,J
0003300 WRITE(6,240) V(1,I),DPDT(1,I)
0003400 30 CONTINUE
0003500 C OUTPUT - VOLTAGE INFO
0003600 WRITE(6,220)FOFF
0003700 WRITE(6,250)
0003800 DO 40 I=1,K
0003900 WRITE(6,260) V(2,I),DPDT(2,I)
0004000 40 CONTINUE
0004100 C MATERIAL IDENTIFICATION AND THICKNESS
0004200 READ(S,115) CMATL
0004300 READ(S,100)THICK
0004400 IF(CMATL.EQ.SMOOTH) GO TO 50
0004500 IF(CMATL.EQ.SUPERH)GO TO 51
0004600 IF(CMATL.EQ.FERRIGO TO 52
0004700 IF(CMATL.EQ.SUPER)GO TO 53
0004800 50 WRITE(6,300)THICK
0004900 WRITE(6,640)
0005000 GO TO 60
0005100 51 WRITE(6,310)THICK
0005200 WRITE(6,630)
0005300 GO TO 60
0005400 52 WRITE(6,320)
0005500 WRITE(6,670)
0005600 GO TO 60
0005700 53 WRITE(6,330)THICK
0005800 WRITE(6,610)
0005900 GO TO 60
0006000 60 CALCULATE CONVERTER OPERATING FREQUENCY
0006100 FREQ=1./(TINC*TJ+TINC*TK)*1.E-6
0006200 WRITE(6,600)FREQ
0006300 DFAD(S,120)
0006400 READ(S,120)
0006500 READ(S,100)
0006600 C CALCULATE SPECIFIC CORE LOSS FOR ON AND OFF WAVEFORMS
0006700 DO 70 I=1,J
0006800 SCL(1,I)=DPDT(1,I)**C*(FON**(-1))
0006900 SCL(2,I)=DPDT(2,I)**C*(FOFF**(-1))
0007000 70 CONTINUE
0007100 TSCL=SCL(1,I)*FON
0007200 TSCL=SCL(2,I)*FOFF
0007300 DO 71 I=1,J
0007400 SCL(2,I)=C*(DPDT(2,I)**C)*(FOFF**(-1))
0007500 SCL(1,I)=SCL(2,I)
0007600 80 CONTINUE
0007700 TSPL=SCL(1,I)*FON
0007800 WRITE(6,500)TSCL
0007900 C CALCULATE TOTAL SPECIFIC CORE LOSS
0008000 TSCL=(TSPL+TSCL)*FON
0008100 WRITE(6,520)TSCL
0008200 FORMT(F70.7)
0008300 FORMT(3)
0008400 FORMT(A1)
0008500 FORMT(E13.3)
0008600 101 FORMAT(1I1,13X,'INPUT DATA FOR HYBRIDIC WAVEFORM ANALYSIS')
0008700 200 FORMAT(' NUMBER OF PRIMARY TURNS',I20,7,'/')
0008800 210 FORMAT(' POSITIVE VOLTAGE EQUIVALENT FREQUENCY',E20.7,' HZ',//)
0008900 220 FORMAT('/-' , ' NEGATIVE VOLTAGE EQUIVALENT FREQUENCY',E20.7,' HZ',//)
0009000 230 FORMAT(' +IVE VOLTAGE-VOLTS',E20.7,'/MAX/SEC',//)
0009100 240 FORMAT(' -IVE VOLTAGE-VOLTS',E20.7,'/MAX/SEC',//)
0009200 240 FORMAT(2E20.7)
0009300 300 FORMAT(1I1,13X,'SPECIFIC CORE LOSS (SCL) FON,FOFF,1', ' SD. ORTHOALI MATERIAL')
0009400 310 FORMAT(1I1,13X,' SD. CORE LOSS (SCL) FON,FOFF,1', ' MIL. SD. FERRITE MATERIAL')
0009500 320 FORMAT(1I1,13X,' SD. CORE LOSS (SCL) FOR FERRITE MATERIAL')
0009600 330 FORMAT(1I1,13X,' SD. CORE LOSS (SCL) FON,FOFF,1', ' SD. SUPERALLOY MATERIAL')
0009700 400 FORMAT(1I1,13X,' SD. PERATING FREQUENCY',E20.7,' HZ')
0009800 500 FORMAT(1I1,13X,' SCL FON',E20.7,' HATT-SEC/LR-CYCLES')
0009900 510 FORMAT(1I1,13X,' SCL FOFF',E20.7,' HATT-SEC/LR-CYCLES')
0010000 520 FORMAT(1I1,13X,' TOTAL SCL',E20.7,' HATT/LR',//)
0010100 600 FORMAT(24X,'*****',//)
0010200 610 FORMAT(17X,'*****',//)
0010300 620 FORMAT(217X,'*****',//)
0010400 630 FORMAT(9X,'*****',//)
0010500 640 FORMAT(17X,'*****',//)
0010600 STOP
0010700 END
EOF

ORIGINAL PAGE IS  
OF POOR QUALITY

```

Figure 21. - Program listing for SCL analysis program.

output formats are shown in Figure 22.

The same example shown in Figure 20 was recalculated using the computer algorithm with the sample interval decreased to 2 μ s. The calculated SCL for this example was calculated as 0.142 watt/pound. This represents an error of only 1.4 percent when compared with the experimentally measured SCL of 0.144 watt/pound.

This example demonstrates that the third method developed in Section 3.4 may be used to determine the SCL for highly distorted waveforms. Also, by decreasing the sample interval the accuracy of the analysis will be improved.

4.3 Examples

In this section five examples are presented which demonstrate the accuracy of the incremental $d\phi/dt$ method. Three magnetic materials were used in the analysis with experimental measurement of their SCL made under both sinusoidal and nonsinusoidal excitation. The waveforms used in these analyses are shown in Figure 23. Both ferrite 3B7 material and Square Permalloy 80 were analyzed using these waveforms. The results of these SCL analyses are shown below:

Material	Sinusoidal excitation		Nonsinusoidal excitation	
	Calculated	Measured	Calculated	Measured
Ferrite	0.388 W/lb	0.369 W/lb	0.244 W/lb	0.247 W/lb
Square Permalloy 80	.777 W/lb	.716 W/lb	.839 W/lb	.831 W/lb

The percentages of error shown for these examples are consistent with those measured for the previous examples. Therefore this method may be used for analysis over the wide range of excitation conditions encountered in the application of the magnetic materials.

OUTPUT FORMAT
INPUT DATA FOR MAGNETIC WAVEFORM ANALYSIS

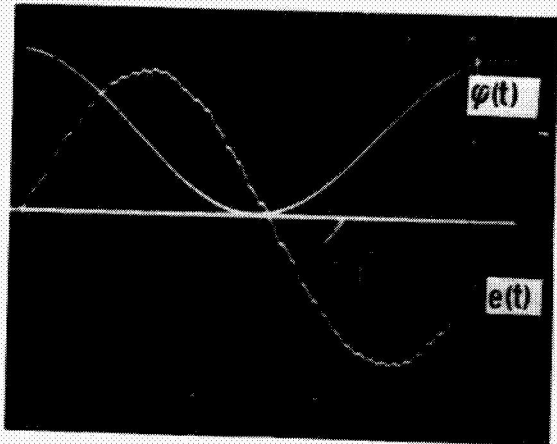
NUMBER OF PRIMARY TURNS= 0.100000E 02

POSITIVE VOLTAGE EQUIVALENT FREQUENCY= 0.1000001E 04 HZ

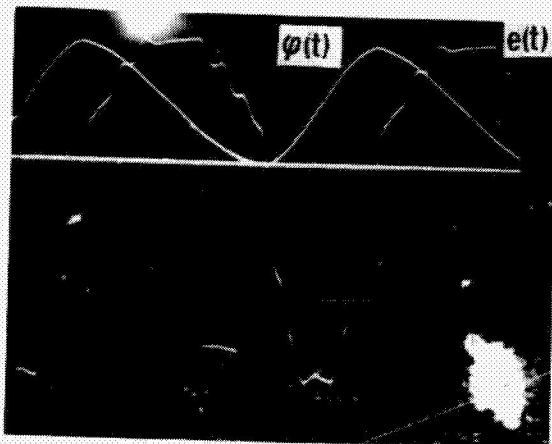
	+IVE VOLTAGE-VOLTS	DP/DT-MAX/SEC
# INPUT FORMAT	0.1763999E 00	0.1764000E 07
# 10. # of turns	0.5132999E 00	0.5133001E 07
# 12 # of +ive sample PTS	0.7995999E 00	0.7996002E 07
# 12 # of -ive sample PTS	0.1007000E 01	0.1007000E 08
# 2. Δt in usec	0.1117000E 01	0.1117000E 08
# .261	0.1117000E 01	0.1117000E 08
# .765	0.1007000E 01	0.1007000E 08
# 1.218	0.7995999E 00	0.7996002E 07
# 1.587	0.5132999E 00	0.5133001E 07
# 1.848	0.1763999E 00	0.1764000E 07
# 1.983	0.1117000E 01	0.1117000E 08
# 1.983 } +e(t) values	0.1007000E 01	0.1007000E 08
# 1.848	0.7995999E 00	0.7996002E 07
# 1.587	0.5132999E 00	0.5133001E 07
# 1.218	0.1763999E 00	0.1764000E 07
# .765	0.1117000E 01	0.1117000E 08
# .261	0.1117000E 01	0.1117000E 08
# .765	0.1007000E 01	0.1007000E 08
# 1.218	0.7995999E 00	0.7996002E 07
# 1.587	0.5132999E 00	0.5133001E 07
# 1.848	0.1763999E 00	0.1764000E 07
# 1.983 } -e(t) values	0.1117000E 01	0.1117000E 08
# 1.983	0.1007000E 01	0.1007000E 08
# 1.848	0.7995999E 00	0.7996002E 07
# 1.587	0.5132999E 00	0.5133001E 07
# 1.218	0.1763999E 00	0.1764000E 07
# .765	0.1117000E 01	0.1117000E 08
# .261 } material type	0.1007000E 01	0.1007000E 08
# 1. tape thickness	0.7995999E 00	0.7996002E 07
# .b30e-13 g - constant	0.5132999E 00	0.5133001E 07
# 2. c } exponents	0.1763999E 00	0.1764000E 07
# .825 u }	0.1117000E 01	0.1117000E 08
-	CONVERTER OPERATING FREQUENCY= 0.1000001E 04 HZ	
SCL ON = 0.6189252E-05 WATT-SEC/LB-CYCLE		
SCL OFF= 0.6189252E-05 WATT-SEC/LB-CYCLE		
TOTAL SCL= 0.1237851E-01 WATT/LB		

SPECIFIC CORE LOSS (SCL) FOR 0.5E 00 JISL SUPERALLOY MATERIAL

Figure 22. - Input-output formats for automated calculation of SCL of a magnetic material.



(a) Sinusoidal excitation.



(b) Nonsinusoidal excitation.

Figure 23. - Waveform excitation for sinusoidal and nonsinusoidal conditions.

ORIGINAL PAGE IS
OF POOR QUALITY

This method may also be used with the square wave SCL characteristics to determine the SCL characteristics for sinusoidal excitation. Figure 24 shows the results of an analysis of a 1000 Hz sine wave for various B_M levels. The calculated results shown as a bold line are compared with the measured sinusoidal characteristics for 1/2 mil Supermalloy material. The results show that an extremely accurate SCL characteristic may be achieved by this method of analysis.

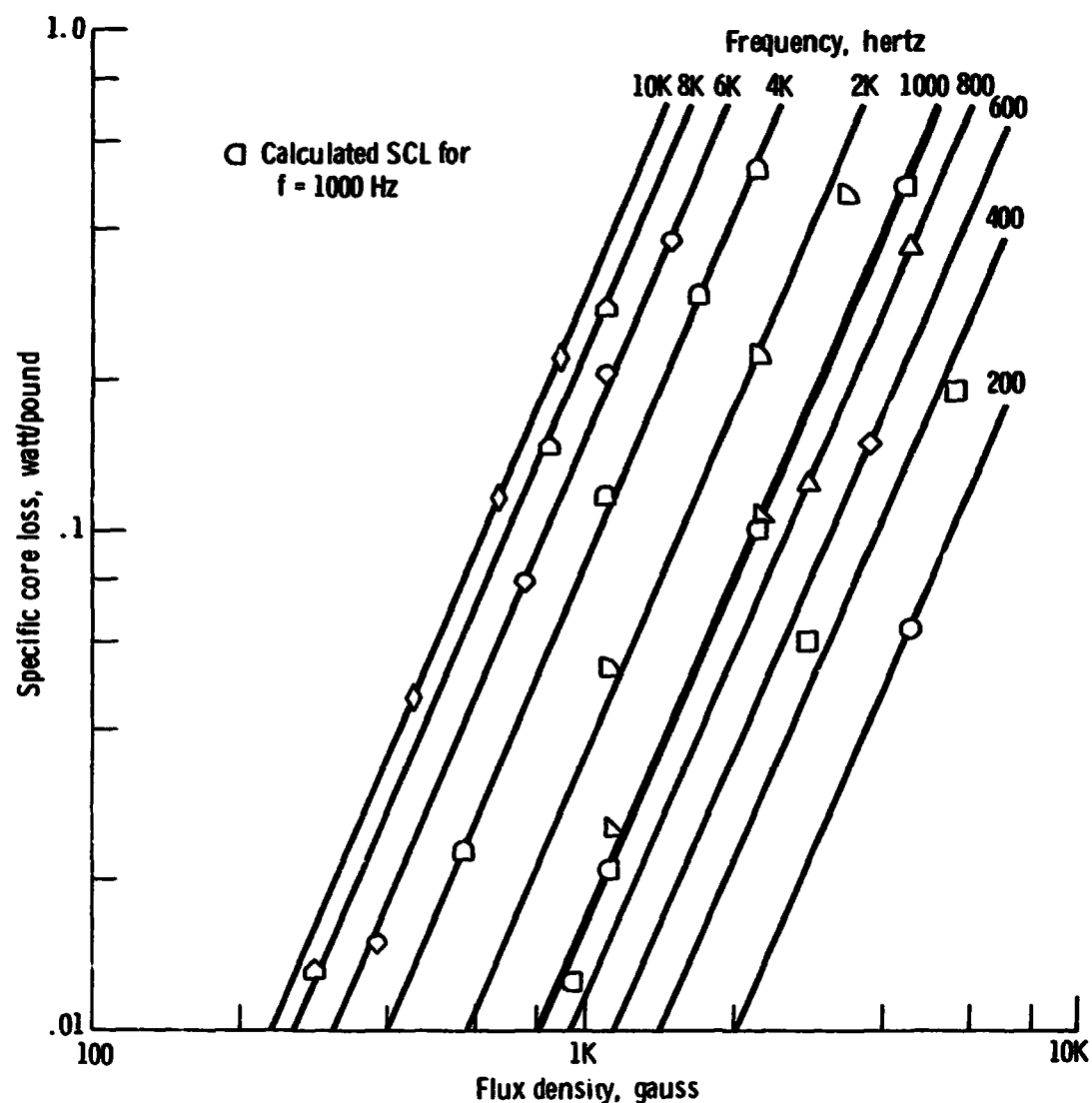


Figure 24. - Comparison of calculated and measured results for specific core loss of 1/2 mil cut Supermalloy under sinusoidal excitation at 1000 Hz.

CHAPTER V

CONCLUSIONS AND SUGGESTIONS FOR FUTURE RESEARCH

5.1 Conclusions

The research covered in this dissertation provides the power electronics designer with a unique analytical tool for investigation of the core loss characteristics of magnetic materials. Analysis methods previously available were based strictly on sinusoidal excitation voltages. Core loss analysis has been based on the assumption that eddy current and hysteresis loss components are separable. By using a novel excitation technique employing a pulse width modulated square wave, a true separation of these two loss components was shown experimentally. This approach provides a straightforward analysis technique to characterize the basic core loss process of new materials (Ref. 27).

For fixed B_M conditions the width of the B-H loop was shown to be a direct function of $d\phi/dt$. If this concept is expanded, a family of B-H curves for various B_M levels may be constructed. Using this family, an operating B-H locus may be constructed for any type of waveform excitation. This approach was used to explain the observed difference in B-H width when excited from either a voltage source (narrow B-H width) or a current source (wider B-H width). The flux characteristics under these two source conditions directly influence the observed B-H shape. For sinusoidal voltage excitation the flux is cosinusoidal in shape and has variable $d\phi/dt$ values over one cycle. For sinusoidal current excitation the flux approaches a

square wave. This excitation causes correspondingly higher $d\phi/dt$ values than those encountered for sinusoidal flux conditions.

These results demonstrate the advantage of using square wave excitation as an analysis tool to determine core loss characteristics. In addition, with square wave excitation the application of Faraday's law becomes straightforward as $d\phi/dt$ is a constant value. The specific core loss characteristics were experimentally measured by holding $d\phi/dt$ constant and varying frequencies to develop a family of core loss characteristics.

In Chapter II the state-of-the-art instrumentation system is discussed. This system was used to obtain large quantities of core loss data quickly and accurately. Through the use of a high power operational amplifier, and three different feedback conditions, current, voltage, and flux sources were easily simulated. This allowed the magnetic characteristics of a large number of source and excitation conditions to be compared and measured easily. With square wave excitation $d\phi/dt$ rates could be calculated directly from excitation voltage levels. A true rms voltmeter was used to measure the excitation voltage level. Accurate core loss was measured for a large number of data points using a wideband wattmeter. This wattmeter has the capability of measuring the power in a 100 kHz square wave to within 2 percent. Instantaneous energy measurements were obtained with a multiplying oscilloscope. A four channel oscilloscope with both time base and X-Y capabilities allowed simultaneous observation of $e(t)$, $i(t)$, $p(t)$, $\phi(t)$, and the B-H loop characteristics of the particular magnetic material under test.

Also in this chapter four different methods for determining stacking factor were covered. Stacking factor error in the published literature is as great as 40 percent. With the measurement methods used in this chapter to determine stacking factor, results consistent to within 5 percent were obtained. Of the four methods used, the oil displacement method yielded the most conservative value for the stacking factor parameter.

Using the SCL characteristics determined under square wave excitation, and the concept of separation of loss variables at constant frequency presented in Chapter III, three analysis techniques were developed which predict the specific core loss of a magnetic material under square wave excitation. The three methods calculated this core loss on the basis of maximum flux density in the core, rate of change of flux within the core, or upon the incremental rate of change of flux in the core.

In Chapter IV the third core loss method was extended to include the analysis of both sinusoidal and nonsinusoidal excitation conditions. To implement the method quickly and reliably, generalized specific core loss equations of the various magnetic materials were derived using experimental data. Once these equations are derived, the specific core losses for various excitation conditions may be readily calculated using a hand calculator. For the examples analyzed in this dissertation a computer algorithm was written to provide a high speed analysis tool which implements the concepts of method three. Analytical core loss predictions compared well with experimentally measured core loss data. These analysis methods are applicable to a broad range of excitation conditions. In addition, the basic SCL charac-

teristics of any desired waveform excitation may be derived.

5.2 Applications in Power Electronics

Most converters in use today excite the magnetic components with some well defined flux waveshape. The emergence of higher power level requirements has led to the development of certain converters using L-C resonant power stages. In these converters the magnetic devices are excited by pseudo-sinusoidal currents. The analysis methods developed in this dissertation are directly applicable to the analysis of the magnetic material behavior under these excitation conditions.

Since all DC-AC/DC converters operate from some steady-state source of raw power, the magnetic exciting voltage as a function of time is a symmetrical or asymmetrical rectangular wave. The exact voltage pulse width is determined by the duty-cycle control mechanism which is incorporated into the converter. In terms of timing implementation, the available duty cycle control schemes are:

Constant on-time T_n , variable off time T_f

Constant T_f , variable T_n

Constant $(T_n + T_f)$, variable individual T_n and T_f

Variable T_n , T_f , and $(T_n + T_f)$

In the examples shown in Chapter III, the duty cycle directly affects the SCL of the magnetic material. Therefore, the magnetic losses associated with these converters are not fixed, but become direct functions of duty cycle. The three SCL analysis methods developed allow detailed performance calculations of the magnetic loss experienced in these converter applications.

5.3 Optimization of Tape Thickness

Using the SCL characteristics of a specific magnetic material

the core loss dependence as a function of tape thickness was investigated. Holding B_M and $d\phi/dt$ constant for the four tape thicknesses measured, it appeared that an optimum tape thickness existed for each of the three magnetic materials tested.

Previous work (Ref. 28) has shown a similar optimization to exist with respect to grain size of the magnetic material. Since the magnetic materials examined in this dissertation were picked from random material batches with uncontrolled grain size, additional controlled experiments using the square wave SCL characteristics as a measure should be performed to examine this observed condition. If a true optimum tape thickness for a given material exists, the traditional practice of using thinner magnetic tapes for higher frequencies would have to be reevaluated.

APPENDIX A

SUMMARY OF SPECIFIC CORE LOSS DATA FOR FERRITE, SUPERMALLOY, AND SQUARE PERMALLOY 80 CORE MATERIALS

The magnetic core loss characteristics are shown in this appendix with SCL (watts/lb) as the dependent variable, and frequency (Hz) as the dependent variable. Flux density (gauss) and $d\phi/dt$ (maxwells/sec) are shown as parameters. While the units given for SCL are not in international units, they are consistent with those used in published data for sinusoidal core loss characteristics. For the tape wound materials tape thicknesses of 1/2, 1, 2, and 4 mils are presented. The ferrite core loss characteristics are for 3B7 material.

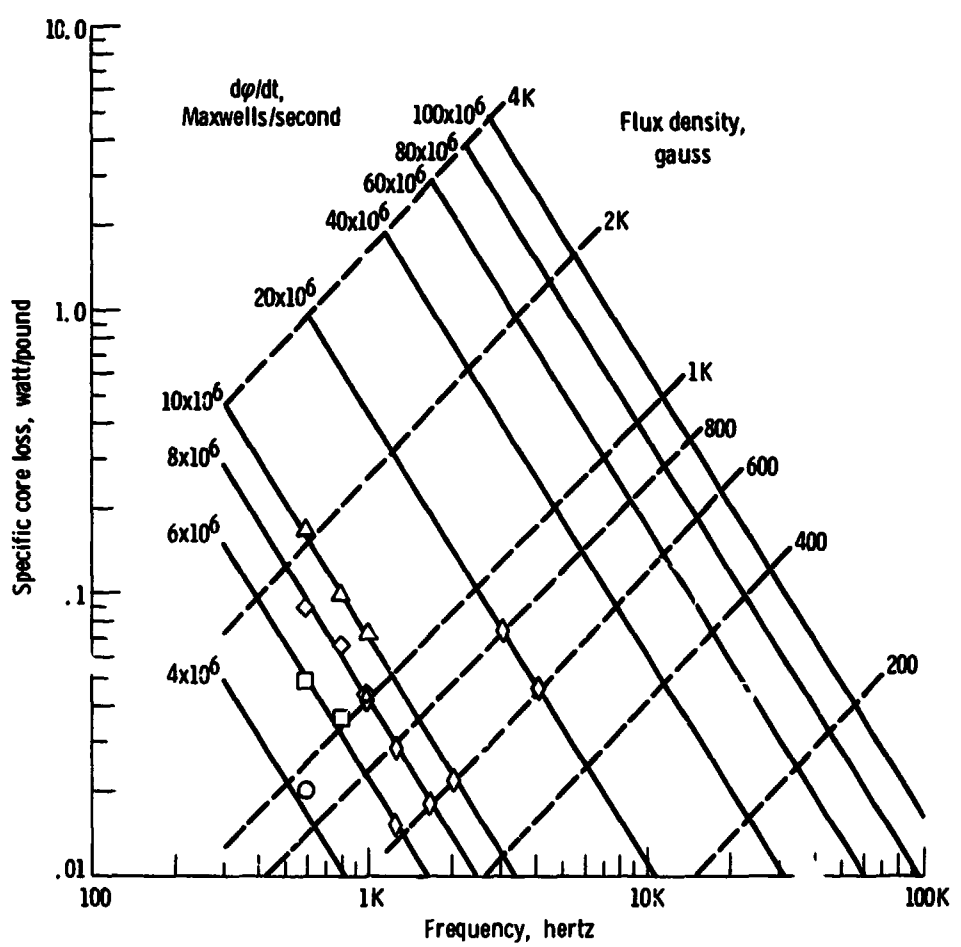


Figure A. 1. - Specific core loss characteristics for 3B7 ferrite.

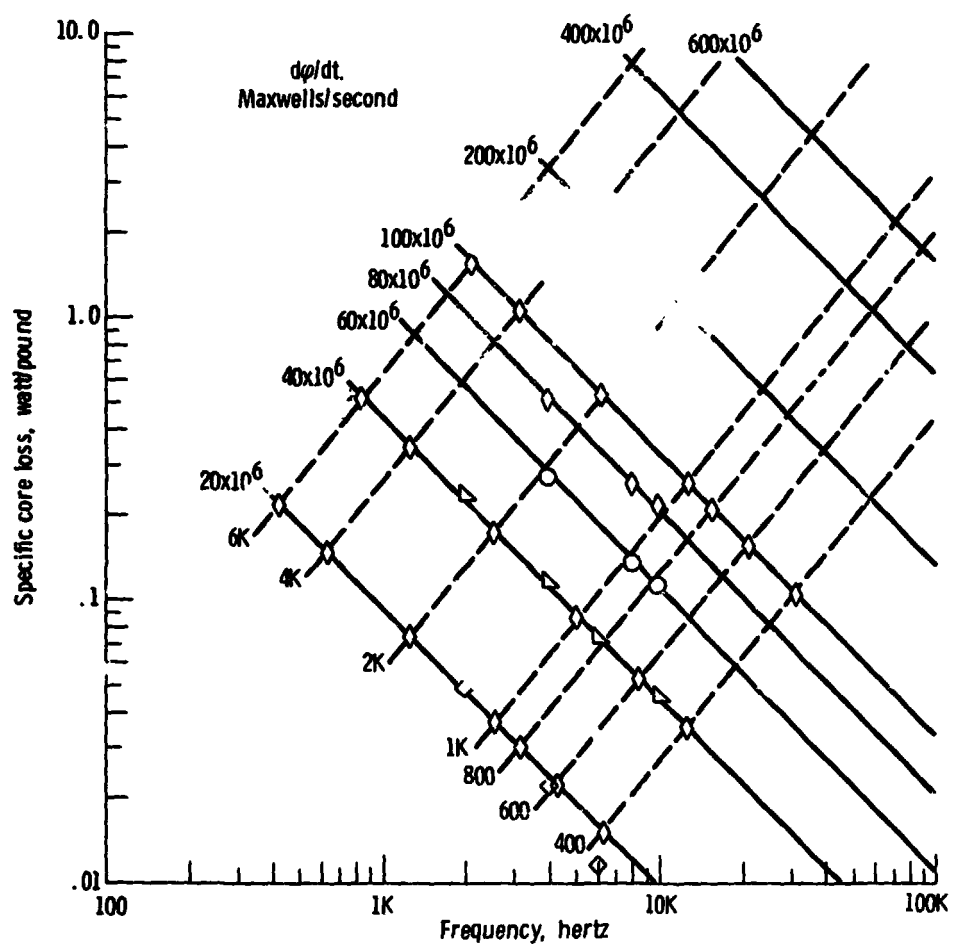


Figure A.2. - Specific core loss characteristics for cut 1/2 mil Supernialloy.

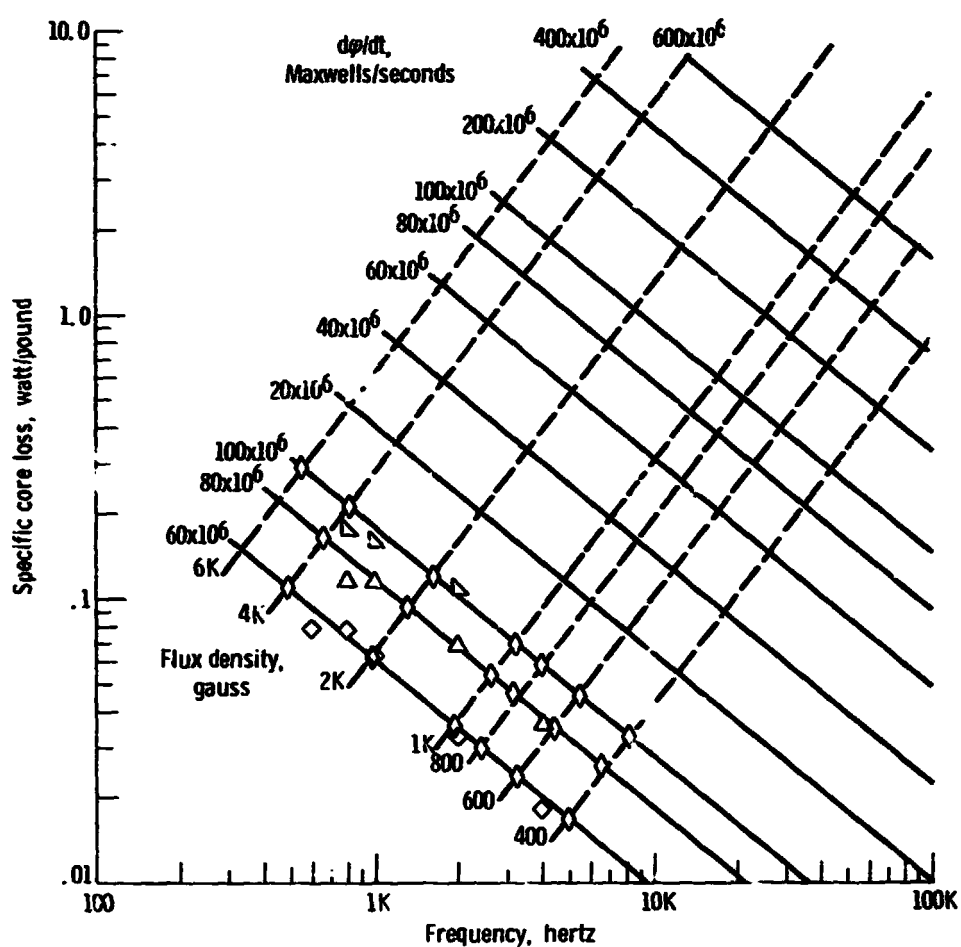


Figure A.3. - Specific core loss characteristics for cut 1 mil Supermalloy.

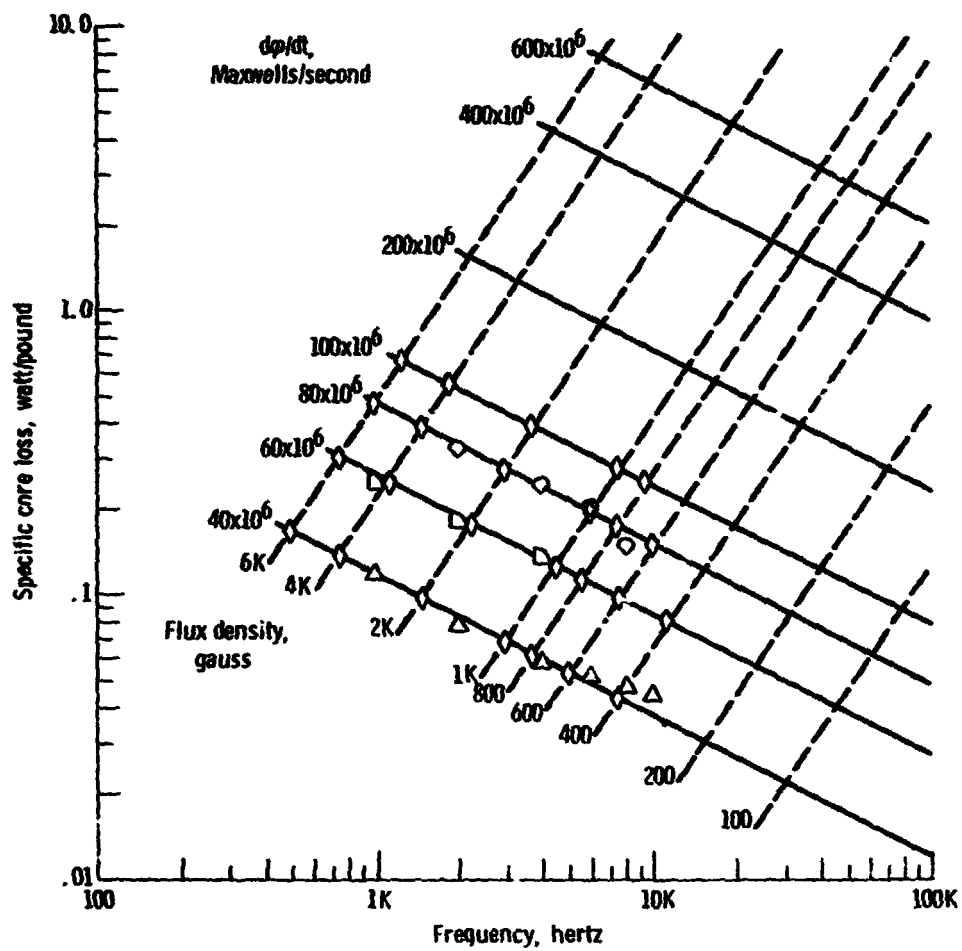


Figure A.4. - Specific core loss characteristics for cut 2 mil Supermalloy.

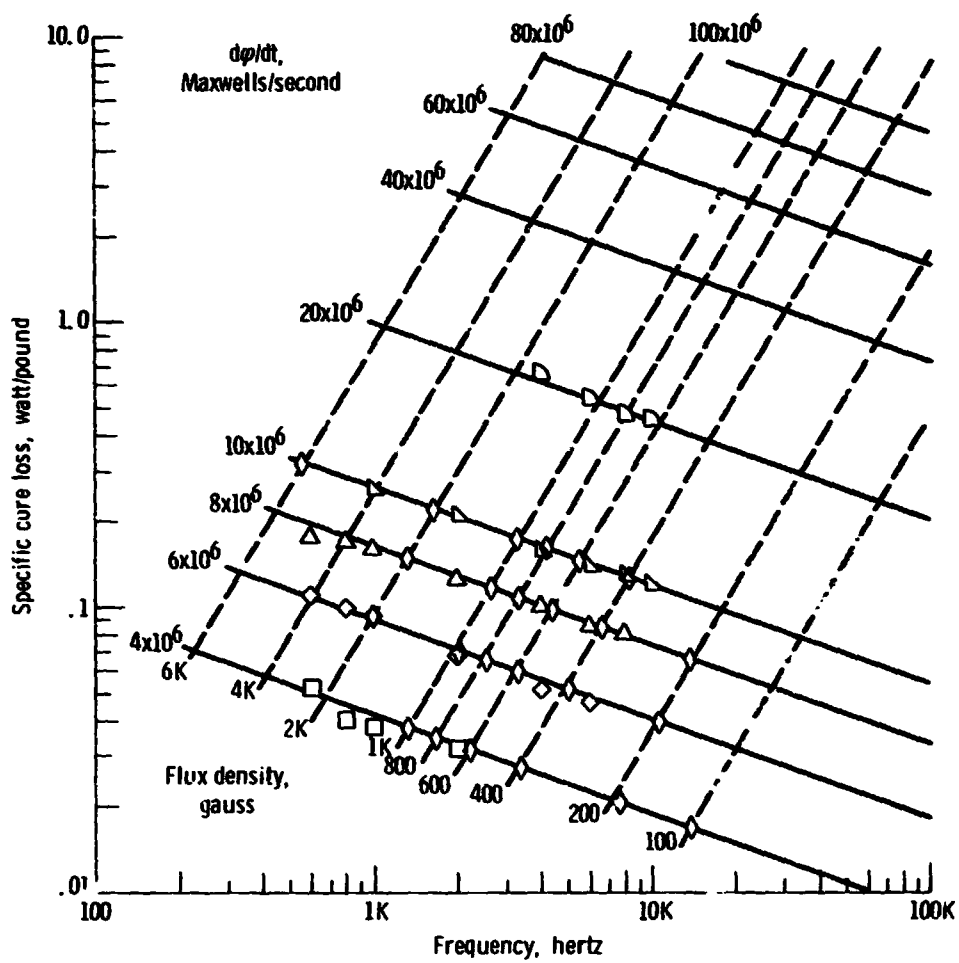


Figure A.5. - Specific core loss characteristics for cut 4 mil Supermalloy.

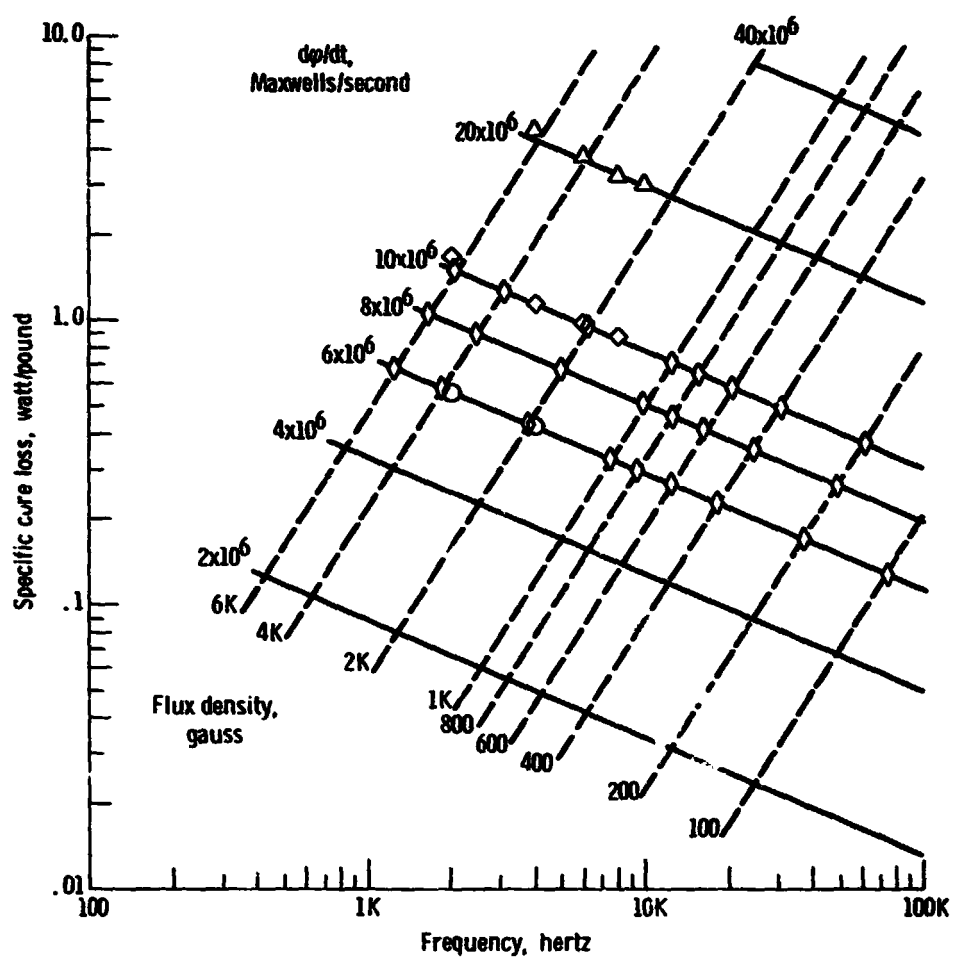


Figure A.6. - Specific core loss characteristics for uncut 1/2 mil Supermalloy.

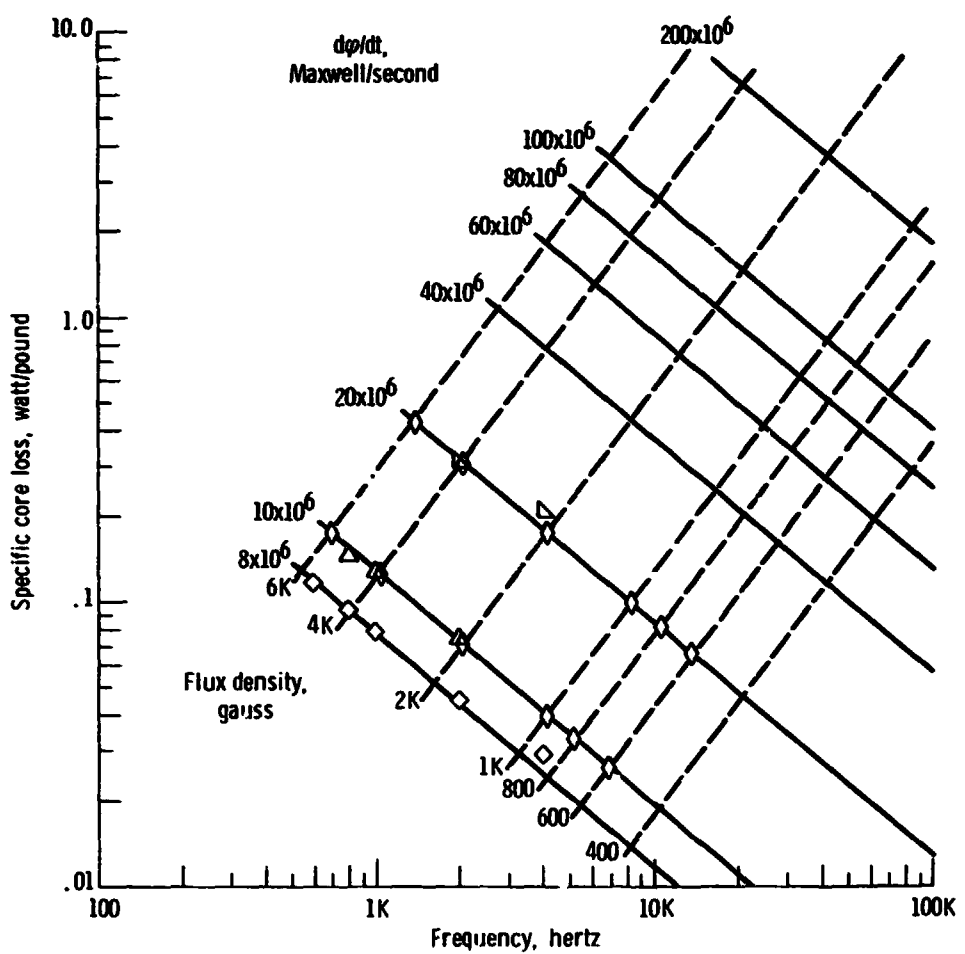


Figure A.7. - Specific core loss characteristics for uncut 1 mil Supermalloy.

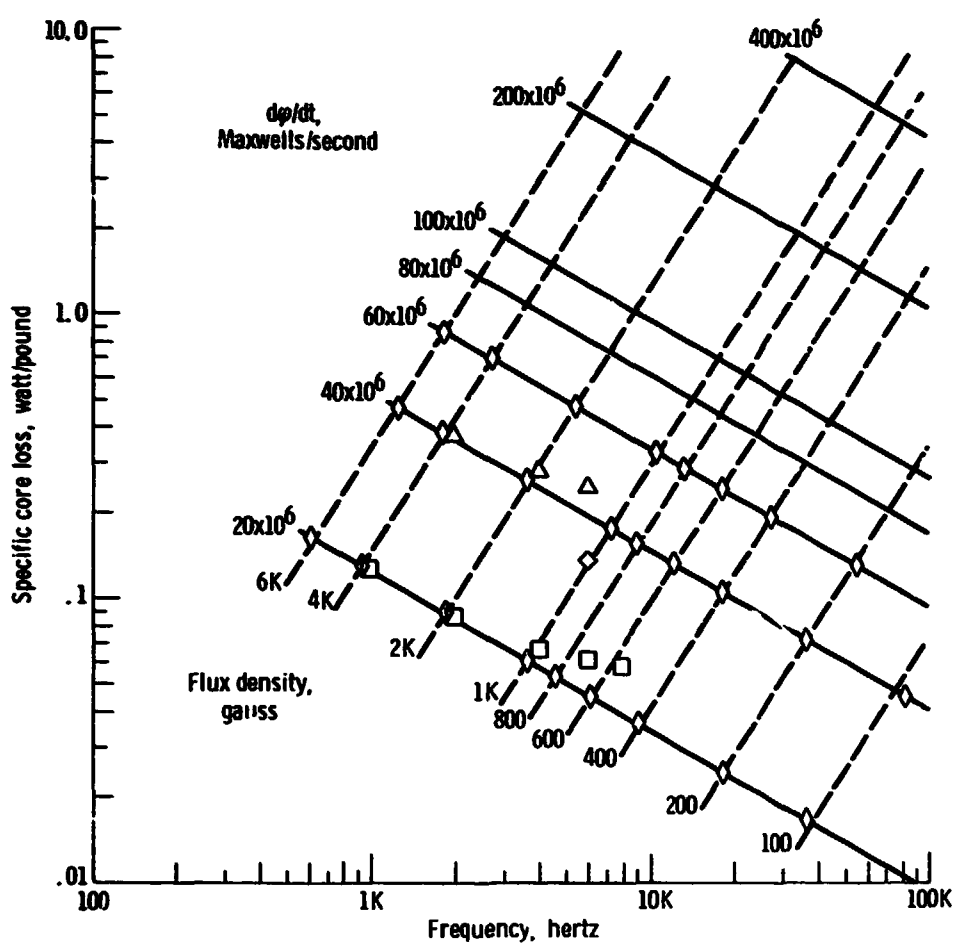


Figure A.8. - Specific core loss characteristics for uncut 2 mil Supermalloy.

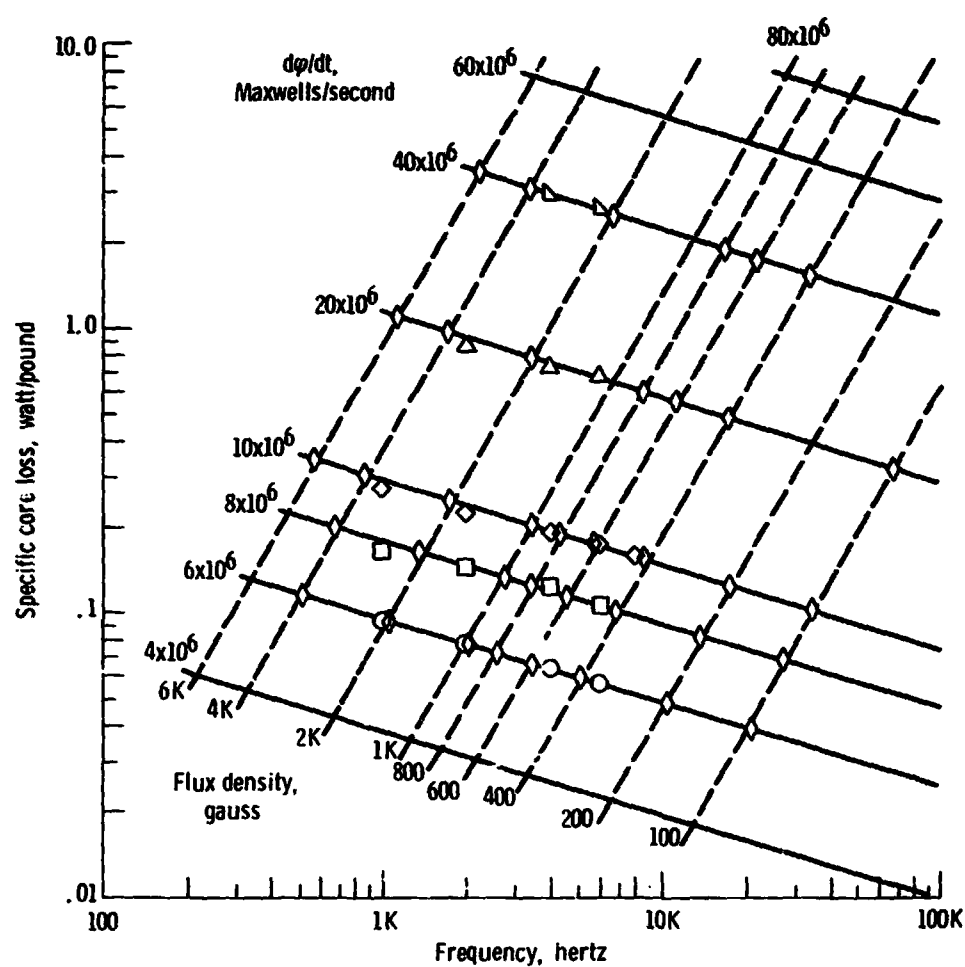


Figure A. 9. - Specific core loss characteristics for uncut 4 mil Supermalloy.

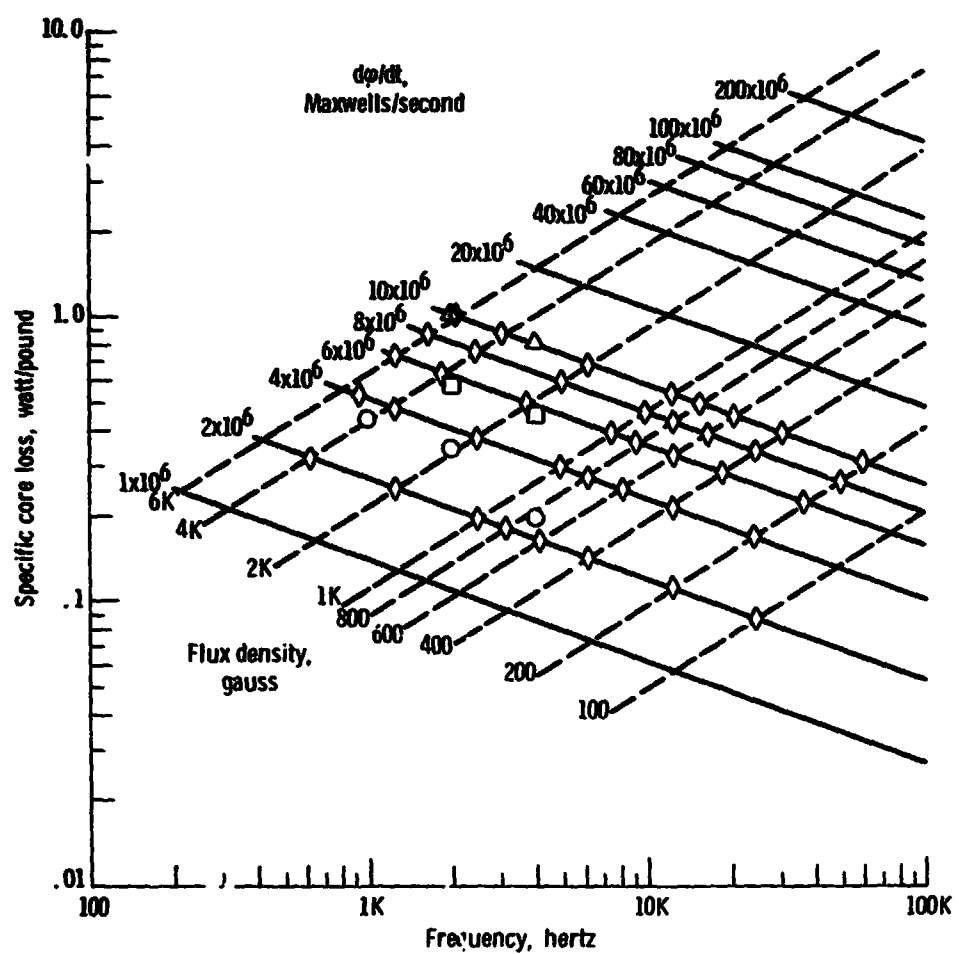


Figure A. 10. - Specific core loss characteristics for uncut 1/2 mil Square Permalloy 80.

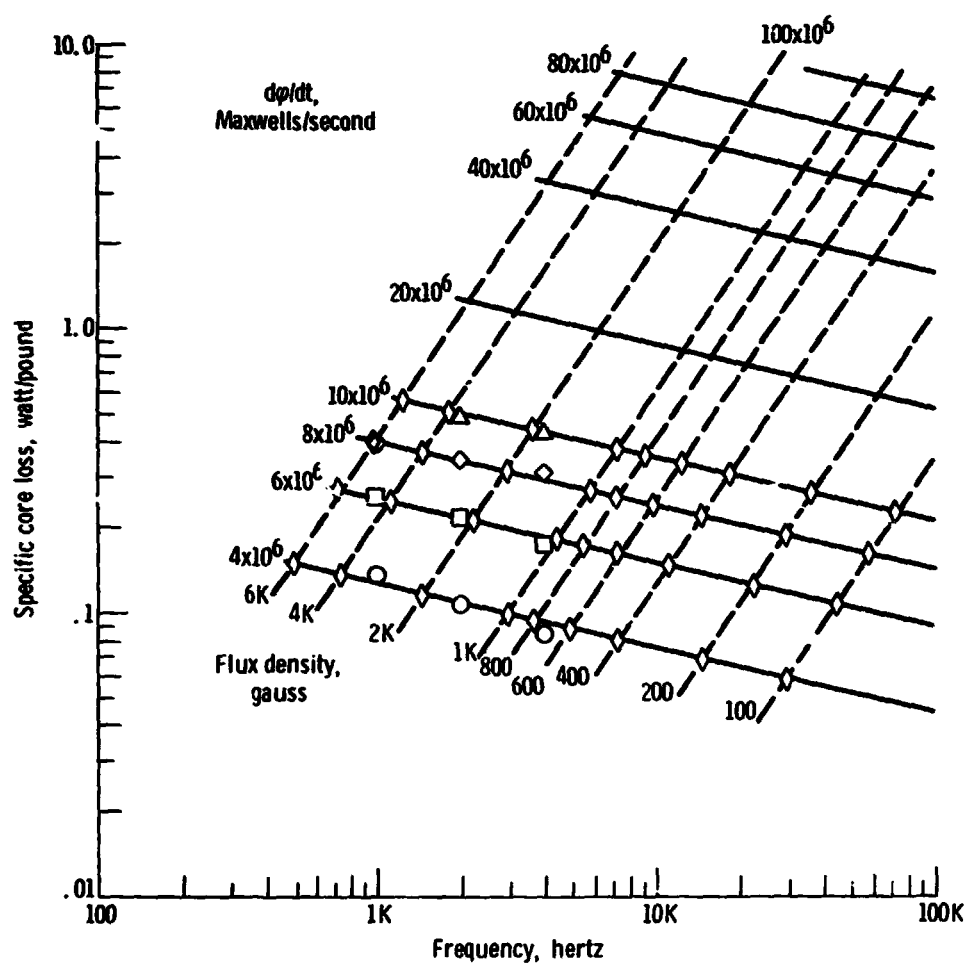


Figure A-21. - Specific core loss characteristics for uncut 1 mil Square Permalloy 80.

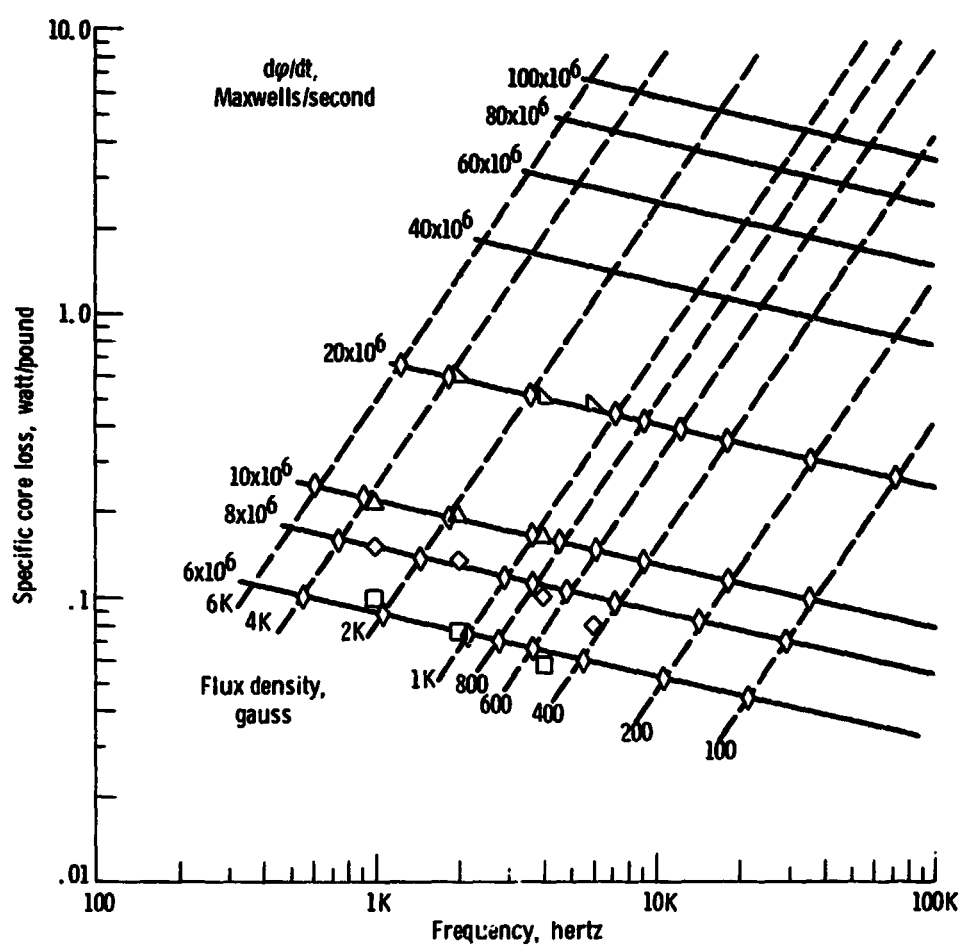


Figure A.12. - Specific core loss characteristics for 2 mil Square Permalloy 80.

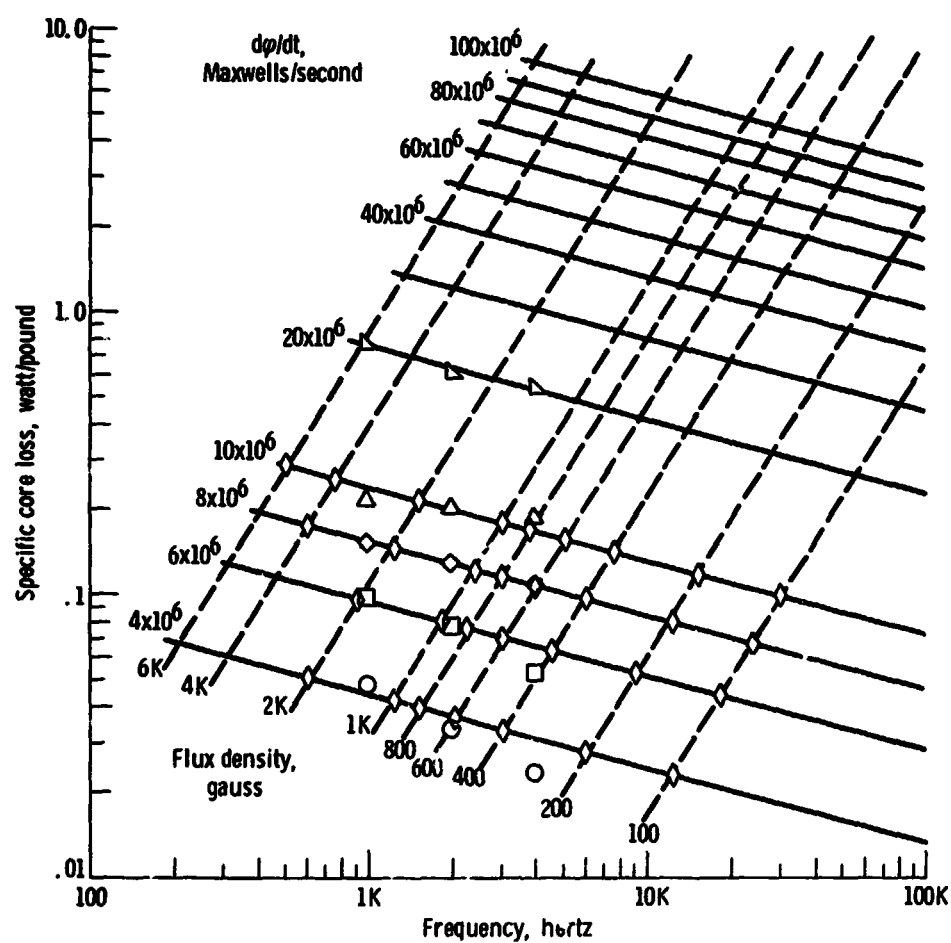


Figure A.13. - Specific core loss characteristics for 4 mil Square Permalloy 80.

APPENDIX B

GLOSSARY OF SYMBOLS

A_c	physical cross sectional area of core, cm^2
A_e	effective cross sectional area of core, cm^2
B	flux density, gauss
B_M	maximum flux density, gauss
$d\phi/dt$	rate of change of flux, maxwells-sec $^{-1}$
$e(t)$	excitation voltage, V
e_c	core voltage, V
$e_i(t)$	input voltage to core sample, V
ΔE_i	incremental energy, W-sec-lb $^{-1}$ -cycle $^{-1}$
E_T	total energy, W-sec-lb $^{-1}$ -cycle $^{-1}$
f	frequency, Hz
f_{eq}^+	positive equivalent frequency, Hz
f_{eq}^-	negative equivalent frequency, Hz
f_{ex}	excitation frequency, Hz
H	magnetizing force,
$i_i(t)$	input current to core, A
k	transformer equation constant
L	mean magnetic path, cm
m	negative half cycle increments
N	number of turns
n	positive half cycle increments
$p_i(t)$	input power to core, W

ρ_{core}	density of core, gm/cm ³
ρ_{oil}	density of oil, gm/cm ³
ϕ	flux, maxwells
ϕ_M	maximum flux, maxwells
$\phi(t)$	instantaneous flux, maxwells
SCL	specific core loss, W-lb ⁻¹
SCL _i	incremental specific core loss, W-lb ⁻¹
SCL _T	total specific core loss, W-lb ⁻¹
SF	stacking factor
Δt_i	incremental time interval, sec
V_{core}	total volume of core structure, cm ³
V_{Fe}	volume of iron, cm ³
$W_{\text{core}}_{\text{air}}$	weight of core in air, gm
W_h	hysteresis loss, J-cycle ⁻¹
ΔW	displacement weight, gm

LIST OF REFERENCES

1. Bozorth, R. M., Ferromagnetism. D. Van Norstrand Co., Inc., 1951.
2. Glasoe, G. N. and Lebacqz, J. V., Pulse Generators. McGraw-Hill Book Co., Inc., 1948.
3. Smit, Jan, Magnetic Properties of Materials. McGraw-Hill Book Co., Inc., 1971.
4. Legg, V. E., "Magnetic Measurements at Low Flux Densities Using the Alternating Current Bridge," Bell System Technical Journal, Vol. 15, No. 1, Jan. 1936, pp. 39-62.
Chen, D. Y., "Comparison of High Frequency Magnetic Core Losses Under Two Different Driving Conditions. A Sinusoidal and a Square-Wave Voltage," I.E.E.E. Power Electronics Specialist Conference, June 1978.
6. Magnetic Inc., Design Manual Featuring Tape Wound Cores. TWC-300R.
7. Hayt, W. H., Jr., Engineering Electromagnetics. McGraw-Hill Book Co., Inc., 1967.
8. Swift, G. W., "Power Transformer Core Behavior Under Transient Conditions," IEEE Transactions on Power Apparatus and Systems, Sept./Oct. 1971, pp. 2206-2210.
9. Warburg, E., "Magnetic Investigations," Ann. Physik Series 3, Vol. 13, 1881, pp. 141-164.
10. Brailsford, F. and Fogg, R., "Anomalous Iron Losses in Cold Reduced Grain-Oriented Transformer Steel at Very Low Frequencies," IEE Proceedings, Vol. 113, No. 9, Sept. 1966, pp. 1562-1564.

11. Swift, W. M., Shilling, J. W., Bhate, S. K., and Young, F. J., "Eddy Current Losses in a (110) [001] Single Crystal of 3% Si-Fe," IEEE Transactions on Magnetics, Vol. MAG-10, April 1974, pp. 810-813.
12. Shilling, J. W. and Houze, G. L., Jr., "Magnetic Properties and Domain Structure in Grain-Oriented 3% Si-Fe," IEEE Transactions on Magnetics, Vol. MAG-10, No. 2, Jun 1974, pp. 195-223.
13. Pry, R. H. and Bean, C. P., "Calculation of Energy Loss in Magnetic Sheet Materials Using a Domain Model," Journal of Applied Physics, Vol. 29, No. 3, Mar. 1958, pp. 532-533.
14. Halliday, D. and Resnick, R., Physics for Students of Science and Engineering. John Wiley & Sons, Inc., 1965.
15. Hollitscher, H., "Core Losses in Magnetic Materials at Very High Flux Densities When the Flux is Not Sinusoidal," IEEE Transactions on Magnetics, Vol. MAG-5, No. 3, Sept. 1969, pp. 642-647.
16. Mitch, J. E., Lewis, H. A., and Parnell, R. A., "Production Testing of Tape Core Materials for Magnetic Amplifiers," AIEE Conference Paper, June 1954.
17. Storm, H. F., Magnetic Amplifiers. John Wiley & Sons, Inc., 1959.
18. Putnam, T. H., "Economics of Power Transformer Design," IEEE Transactions on Power Apparatus and Systems, Vol. 82, No. 12, Dec. 1963, pp. 1018-1023.
19. Lee, F. C., Yu, Y., and Triner, J. E., "Power Converter Design Optimization," IEEE Transactions on Aerospace and Electronic Systems, Vol. AES-15, No. 3, May 1979, pp. 344-355.

C - C

20. Alexanderson, E. F. W., "Magnetic Properties of Iron at Frequencies up to 200,000 Cycles," AIEE Journal, Vol. XXX, Part III, 1911, pp. 2433-2454.
21. Boon, S. C. and Robey, J. A., "Effect of Domain Wall Motion on Power Loss in Grain Oriented Silicon-Iron Sheet," IEEE Proceedings, Vol. 115, No. 10, Oct. 1968, pp. 1535-1540.
22. Overshott, K. J., "The Use of Domain Observations in Understanding and Improving the Magnetic Properties of Transformer Steels," IEEE Transactions on Magnetics, Vol. MAG-12, No. 6, Nov. 1976, pp. 840-845.
23. Lauers, J. D., Biringer, P. P., and Hollitscher, H., "A Simple Method of Estimating the Minor Loop Hysteresis Loss in Thin Laminations," IEEE Transactions on Magnetics, Vol. MAG-14, No. 5, Sept. 1978, pp. 386-388.
24. Lauers, J. D. and Biringer, P. P., "Prediction of Core Losses for High Flux Densities and Distorted Flux Waveforms," IEEE Transactions on Magnetics, Vol. MAG-12, No. 6, Nov. 1976, pp. 1053-1055.
25. Lauers, J. D., Biringer, P. P., and Hollitscher, H., "Estimation of Core Losses When the Flux Waveform Contains the Fundamental Plus a Single Odd Harmonic Component," IEEE Transactions on Magnetics, Vol. MAG-13, No. 5, Sept. 1977, pp. 1128-1130.
26. Ward, W. P., Introduction to Electrical Engineering. Prentice Hall, Inc., 1952.
27. Chen, D. Y., "Amorphous Magnetic Alloys for High Frequency Power Electronic Applications," IEEE Power Electronics Specialist Conference, June 1979.

28. Overshott, K. J. and Thompson, J. E., "Magnetic Properties of
Grain Oriented Silicon Iron. Part 4 - Relationship of Domain
Spacing, Grain Size, Sheet Thickness, and Power Loss," Pro-
ceedings of the IEE, Vol. 117, No. 4, Apr. 1970, pp. 865-868.

BIOGRAPHY

Name: [REDACTED]

Date of Birth: [REDACTED]

Place of Birth: [REDACTED]

Universities attended:	Dates	Degree	Dates of degree
Cleveland State University	1965-1969	B.E.E.	June, 1969
University of Toledo	1969-1974	M.S.E.E.	March, 1974
University of Toledo	1974-1979	Ph.D.	August, 1979

Major: Electrical Engineering

Minor: Engineering Science and Mathematics

Publications:

1. _____, "A Digital Regulated Solar Array Power Module," NASA TM X-2314, July 1971.
2. _____, with R. P. Iwens and Y. Yu, "Time Domain Modeling and Stability Analysis of an Integral Pulse Frequency Modulated DC to DC Power Converter," IEEE Power Electronics Specialist Conference, 1975 Record, pp. 80-90, IEEE Publication 75 CHO 965-4AES.
3. _____, with Y. Yu, M. Bachmann, and F. C. Lee, "Formulation of a Methodology for Power Circuit Design Optimization," IEEE Power Electronics Specialist Conference, 1976 Record, pp. 35-44, IEEE Publication 76-CHI 084-3 AES.

4. _____, with F. C. Lee and Y. Yu, "Modeling of Switching Regulator Power Stages With and Without Zero-Inductor-Current Swell Time," IEEE Power Electronics Specialist Conference, 1976 Record, pp. 62-72, IEEE Publication 76-CHI 084-3 AES.
5. _____, with I. G. Hansen, "Electric Vehicle Power Train Instrumentation - Some Constraints and Considerations," International Electric Vehicle Exposition (IEVE), April 1977.
6. _____, with R. P. Iwens and F. C. Lee, "Discrete Time Domain Modeling and Analysis of DC-DC Converters with Continuous and Discontinuous Inductor Current," Second IFAC Symposium on Control in Power Electronics and Electrical Drives, October 1977.
7. _____, with F. C. Lee, R. P. Iwens, and Y. Yu, "Generalized Computer Aided Discrete Time-Domain Modeling and Analysis of DC-DC Converters," IEEE Transactions on Industrial Electronics and Control Instrumentation, Vol. IECL-26, No. 2, May 1979, pp. 58-69.
8. _____, with Y. Yu, and F. C. Y. Lee, "Power Converter Design Optimization," IEEE Transactions on Aerospace and Electronic Systems, Vol. AES-15, No. 3, May 1979, pp. 344-355.

Positions Held:

1. Teaching Assistant, Cleveland State University, 1967-1969.
2. Aerospace Engineer, NASA Lewis Research Center, 1969-present.

Membership in Honorary Societies:

Eta Kappa Nu

Pi Mu Epsilon